The Effects of Trabecular Architecture, Strength, and Bone Mineral Density on Calcaneal Ultrasound

by

Stefan E. Radloff

B.S., Mechanical Engineering
University of Tulsa, 1993

Submitted to the Department of Mechanical Engineering
in Partial Fulfillment of the Requirements for the
Degree of

Master of Science in Mechanical Engineering

at the
Massachusetts Institute of Technology
January 1995

Signature of Author.....
Department of Mechanical Engineering
January, 1995

Certified by .....
Wilson C. Hayes, Ph.D.
Thesis Advisor

Accepted by .....
Ain A. Sonin, Ph.D.
Chairman, Departmental Committee on Graduate Studies

The Effects of Trabecular Architecture, Strength, and Bone Mineral Density on Calcaneal Ultrasound

by

Stefan E. Radloff

Submitted to the Department of Mechanical Engineering
on January 20, 1995 in Partial Fulfillment of the Requirements for the
Degree ofMaster of Science in Mechanical Engineering

Abstract

With our increasing life spans and growing elderly population osteoporosis has become an important public health issue. Osteoporosis, a decrease in bone mass, results in a significant increase in bone fragility and susceptibility to bone fracture. Osteoporosis currently affects more than 25 million people in the United States, resulting in 1.3 million fractures annually.

Quantitative ultrasound of the calcaneus has recently been introduced as a technique for assessing skeletal status that may provide advantages over the current techniques. Several investigators have shown that quantitative ultrasound of bone in vitro correlates with bone density, elastic modulus, and bone strength. However, ultrasound measurements in vivo are only moderately correlated with bone density. Therefore, it has been suggested that ultrasound measurements are influenced by the morphology of trabecular bone. To address these issues, we have investigated the following questions: 1) Do quantitative ultrasound measures of human trabecular bone specimens from the calcaneus, as well as ultrasound measures of intact cadaveric feet correlate with trabecular bone morphology?; 2) Do quantitative ultrasound measures of human trabecular bone specimens from the calcaneus, as well as quantitative ultrasound of intact cadaveric feet correlate with the mechanical properties of the trabecular bone?, 3) Does quantitative ultrasound provide information about either the trabecular bone morphology or mechanical properties that is independent of bone density?

To answer these questions, we assessed broadband ultrasound attenuation and speed of sound in intact cadaveric feet and trabecular bone specimens removed from the calcaneus. Bone density was measured by dual-energy x-ray absorptiometry and computed tomography. To evaluate trabecular morphology we performed micro-magnetic resonance imaging on the trabecular bone specimens. Mechanical testing was performed to determine the elastic moduli and ultimate strength of the trabecular bone. Finally, the mechanical properties, as well as the ultrasonic, density, and morphology parameters were compared.

We found that most trabecular bone morphology parameters are correlated to ultrasound of trabecular bone specimens and intact cadaveric feet. With two exceptions, density was better correlated to morphology than ultrasound. In most cases, a combination of ultrasound and density parameters did not explain the variation of morphology better than density alone.

We also found that quantitative ultrasound of both trabecular bone specimens and intact cadaveric feet are correlated to the mechanical properties of calcaneal trabecular bone. This was especially true for the ultimate strength of trabecular bone, which was

moderately to highly correlated to ultrasound measures. In most cases, a combination of ultrasound and density did not explain variations in the mechanical properties better than density alone.

Our data suggests that quantitative ultrasound of the calcaneus may be little more than a different way to measure bone density. Density was usually the best predictor of trabecular morphology or mechanical properties, occasionally quantitative ultrasound was the best predictor. The combination of ultrasound and density parameters did not improve the predictions of trabecular morphology or mechanical properties by clinically significant levels.

Thesis Supervisor: Wilson C. Hayes, Ph.D.

Title: Professor of Biomechanics, Harvard - MIT Division of Health Sciences and Technology, Massachusetts Institute of Technology

Acknowledgements

There are countless people that I owe my thanks to:

Mary Bouxsein, for her help, insights, guidance, and advice. I could not have completed this project without her. Mary kept me, thankfully, both playing and working.

Toby Hayes, for believing in me and supporting me.

The members of the Orthopaedic Biomechanics Lab, especially Tania, Rick, Em, Craig, Deb, Aaron, Dave, Ann, Aya, Matt, Talya, Jeanine, and Paula

Michael Harrington, for his help with the computers, day and night.

John Hipp and Dan Michaeli, for their help with AVS and the morphology routines.

John Henshaw, University of Tulsa, and Alan Morimoto, Sandia National Laboratories, for their encouragement and advice in the beginning.

Sam Gravina and Bruker Instruments, for use of the microMRI and the cheerful assistance that always came with it.

My parents, who have always given me their unquestioning support.

Support was provided by the M. E. Müller Professorship in Biomechanics, NIH, and an equipment grant from Walker Sonix, Inc.

Table of Contents

Chapter 1 - Introduction

With our increasing life spans and growing elderly population osteoporosis has become an important public health problem. Osteoporosis is a skeletal disease characterized by low bone mass and microarchitectural deterioration of bone tissue, resulting in a significant increase in bone fragility and susceptibility to bone fracture. Osteoporosis currently affects more than 25 million people in the United States (Anonymous, 1993), resulting in 1.3 million fractures annually (Melton, 1988). Over 280,000 of these fractures are hip fractures, resulting in medical costs approaching $10 billion annually (Anonymous, 1993). One third of women over the age of 65 will experience a vertebral fracture (Melton *et al.* 1989). Age - related fractures present not only an economic burden, but also dramatically impair individuals' quality of life, leading to reduced mobility, loss of independence, and increased mortality. By the middle of the next century it is predicted that increases in life expectancy will cause fracture incidence to increase by a factor of three (Anonymous, 1993).

Several factors contribute to age related fracture, including reduction in bone density as a result of osteoporosis, fall configuration, and physical dysfunctions that lead to falls. Women with femoral neck bone density one standard deviation below the mean are 2.6 times more likely to fracture their hip than a women with average bone density for her age (Cummings *et al.* 1993). The detection and treatment of low bone density, as well as an increased understanding and prevention of falls may help lower the rate of age related fractures, thereby reducing health care costs and increasing the quality of life for the elderly.

Current methods to diagnose and measure bone loss include single- (SPA) and dual-photon (DPA) absorptiometry, single- (SXA) and dual-energy x-ray absorptiometry (DXA), and computed tomography (CT). Each method involves the use of ionizing radiation. Quantitative ultrasound (QUS) of the calcaneus is a relatively new technique

that is currently being investigated as a potential diagnostic and screening tool for fracture risk. QUS measures the attenuation and velocity of ultrasound as it passes through the calcaneus, or heel bone. Several studies have shown that QUS measurements are correlated with bone density (Baran, 1991; Gluer *et al.* 1992; Salamone *et al.* 1994). However, a significant part of the variation in the ultrasound data is not explained by bone density. Therefore, it has been suggested that ultrasound measurements are influenced by the microstructure of trabecular bone in the heel (Gluer *et al.* 1993; Kaufman, Einhorn, 1993). Thus, the goal of this research was to determine whether ultrasound velocity and attenuation measures of the intact foot are associated with the morphology of calcaneal trabecular bone. Furthermore, we asked whether this association is independent of the density of the trabecular bone.

Once the technique is understood, use of QUS to screen for osteoporosis and fracture risk has advantages over the current methods. QUS is inexpensive, giving many people access to the technology. Also, unlike the other techniques, QUS is radiation free. The device is small and portable, allowing for office - based testing. Finally, QUS may measure some aspect of bone architecture in addition to bone density, providing more information to the clinician than conventional techniques. These factors, combined with early testing and diagnosis of fracture risk, could combine to help reduce the incidence of age related fracture, resulting in reduced health care costs and better quality of life for many people.

Historical Background of Ultrasound Assessment Techniques

Sound is a mechanical disturbance that propagates through a medium as a wave. A sound wave is defined by its velocity, frequency, and amplitude. Frequency, expressed in Hertz (Hz), is the number of times per second the particles in the medium oscillate back and forth as a result of the disturbance. Amplitude is the magnitude of this disturbance. Velocity is the product of frequency and wavelength ($v = f$). Humans can hear sound in

the frequency range from 20 to 20,000 Hz, while ultrasound is defined as mechanical energy oscillating at frequencies above 20,000 Hz.

In contrast to x-rays, the development of ultrasound was slow and fraught with technological difficulties (Holmes, 1974). Ultrasound waves are produced by piezoelectric crystals, crystals that vibrate in response to electrical stimulation. The piezoelectric effect and ultrasound were discovered in 1880 by Pierre and Jacques Curie (Taube, Adelstein, 1987). At first, ultrasound was used to locate submerged bodies. For example, in 1912 ultrasound was used in an unsuccessful attempt to locate the sunken Titanic (Holmes, 1974). During World War I ultrasound was used to locate submarines (Taube, Adelstein, 1987). The technology did not progress significantly until the 1920's when the vacuum tube and improved piezoelectric sources were developed (Taube, Adelstein, 1987).

The first medical use of ultrasound came in 1937, when K.T. Dussek of Austria designed and developed a crude device to image cerebral ventricles and intracranial tumors (Bushong, Archer, 1991). World War II brought about more advanced use of ultrasound with the development of SONAR, sound navigation and ranging. The equipment and technology developed during the war stimulated further research in medical ultrasound. In the 1950's John Wild was able to measure intestinal wall thickness with ultrasound. Wild was one of the first to use ultrasound as a technique for both anatomical imaging and as well as characterization of tissue, primarily for the diagnosis of breast tumors. Wild demonstrated that ultrasound could discriminate between normal and cancerous tissue (Wild, Reid, 1952; Taube, Adelstein, 1987). At approximately the same time Douglass Howry at the University of Denver developed a successful second generation system for soft tissue imaging (Holmes, 1974). Despite many successes, ultrasound imaging still had some setbacks. In 1955 the United States Atomic Energy Commission declared that "there is no possibility of adapting this (ultrasonics) to detecting intracranial lesions for even if the skull did not have high absorption properties of its own,

the distances involved would make the application foolish." (Brown, 1975). However, by 1960 ultrasound systems for imaging soft tissue were commercially available (Bushong, Archer, 1991). Today diagnostic ultrasound is used in a wide variety of applications at frequencies ranging from 1 to 15 MHz; from echocardiography to imaging of blood flow using Doppler ultrasound (Brown, 1975).

Clinical Measurements in Quantitative Ultrasound Assessment of Bone

Ultrasound is frequently used for the structural evaluation of conventional engineering materials such as steel or concrete (1987), while the use of ultrasound as a technique for assessing fracture risk in bone is relatively new. Two parameters are used to measure bone status using ultrasound: attenuation and velocity. To make these measurements the bone and surrounding tissue is placed between two ultrasound transducers. Each transducer both sends and receives ultrasound signals. The transducers can be placed in contact with the tissue or bone surface by using an acoustic coupling medium. Alternatively, water can be used as a sound transmission medium between the ultrasound transducers and the tissue surface.

To characterize bone, the attenuation and velocity measures have been further refined. Two attenuation parameters: broadband ultrasound attenuation and average ultrasound attenuation, and three velocity parameters: bone velocity, heel velocity, and speed of sound, are commonly obtained from QUS of the calcaneus. Broadband ultrasound attenuation (BUA) is not a direct measure of ultrasound attenuation, but rather it reflects the frequency dependence of the ultrasound attenuation. Attenuation, or energy loss, of the ultrasound signal as it passes through tissue and bone is measured at many frequencies in the range from 0.20 to 0.60 MHz. BUA is defined as the slope of the attenuation vs. frequency curve with units of dB/MHz.

The second, less common of the two attenuation measures is average ultrasound attenuation (AUA). AUA is simply the average attenuation of ultrasound over a range of frequencies. The same frequency range that is used to evaluate BUA is used to calculate AUA. To date, ultrasound research has focused primarily on BUA and velocity measures, whereas examination of AUA has been limited.

Three different ultrasound velocity measurements can be made: speed of sound (SOS), bone velocity (BV), and heel velocity (HV). SOS is the velocity of the ultrasound wave as it travels from one transducer to the other. HV is the velocity through the heel, including both bone and soft tissue. Finally, BV is the velocity of ultrasound through only the calcaneus. The three velocity measurements are shown below in Figure 1-1.

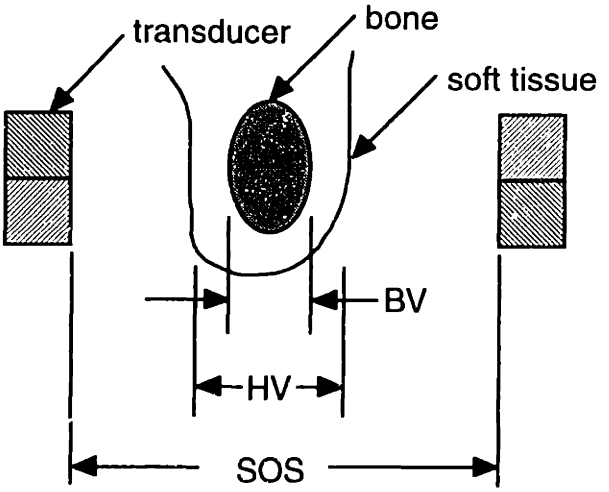

Figure 1-1 QUS velocity measurements: bone velocity (BV), heel velocity (HV), and speed of sound (SOS)

Ultrasound systems calculate bone and heel velocity by measuring the ultrasound wave that is reflected off of the water - tissue or tissue - bone interface. It is not yet known which velocity measure will provide the best clinical utility. Miller *et al* (1993) concluded that HV is the best parameter for a QUS system where the ultrasound transducers are placed in direct contact with the tissue surface, while SOS is the optimum parameter for a water - based system. Their conclusions were based on the precision and range of each velocity parameter using a contact QUS machine. These parameters will vary among

manufacturers, subject groups, and even different machines, so Miller's conclusions are not necessarily universally applicable. It was shown that the three velocity measures are highly correlated with each other (Miller *et al.* 1993), indicating that three different measurements may not be more meaningful than a single velocity measurement.

The site most commonly used for QUS measurements is the calcaneus, or heel bone. The calcaneus is used for several reasons: 1) the foot is easily accessible; 2) the sides of the heel and the calcaneus are roughly parallel, minimizing energy loss of the ultrasound wave due to reflection and refraction as the wave passes through the foot; and 3) the calcaneus is comprised primarily of trabecular bone with a thin shell of cortical bone. The presence of trabecular bone is important because the reduction of bone mass observed in women or men with osteoporosis is evident first in trabecular bone. Furthermore, in a study comparing the bone mineral content (BMC) at four different sites (calcaneus, proximal and distal radius, and lumbar spine) with the subsequent incidence of fracture, bone mineral content of the calcaneus was the best predictor of fracture incidence (Wasnich *et al.* 1987).

Theory of Ultrasound Velocity and Attenuation in Bone

The underlying theory explaining the propagation of ultrasound through trabecular bone is not well understood. Two factors lead to the attenuation of ultrasound: scattering and absorption. Scattering is caused by refraction and reflection of the ultrasound wave as it passes boundaries between materials of varying densities. Absorption is caused primarily be thermal losses, and increases with increasing frequency of the wave. Recently the Biot theory (Biot, 1994; Biot, 1962; Biot, 1962) has been used in an attempt to describe ultrasound attenuation in bone (McKelvie, Palmer, 1994; Williams, 1992). In 1956 Biot proposed a theory to explain ultrasound propagation in porous rocks and sediment for geophysical testing (Biot, 1994). However, the theory applies to ultrasound propagation in any inhomogenous material. McKelvie *et al* (1994) established that the

Biot theory can qualitatively predict the attenuation behavior of ultrasound in normal and osteoporotic bone. However, their quantitative results of ultrasound velocity did not agree with in vitro tests of human calcaneal bone specimens. Experimental results showed that velocity decreased in osteoporotic bone, while the calculated velocity using Biot theory increased (McKelvie, Palmer, 1994). Williams (1992) achieved better results using the Biot theory to predict the velocity of ultrasound in bovine bone. He reported a correlation coefficient of $r = 0.78$ between experimental ultrasound velocity and velocity predicted using the Biot theory (Williams, 1992). Although use of the Biot theory is an important step leading to the theoretical understanding of the behavior of ultrasound in bone, more work is required to achieve a good understanding of the behavior of ultrasound in bone.

Development of Ultrasound Velocity to Assess Structural Properties of Bone

Ultrasound velocity was first used to determine the material properties of bone. Direct in vitro measurement of the modulus of elasticity of bone is possible because the velocity of an ultrasonic wave through a homogeneous material is dependent on the elastic modulus and density of the material. The relationship is expressed as:

$$v = \sqrt{E/\rho}$$

Lang (1970) was one of the first to determine the modulus of elasticity of bone using ultrasound, confirming that bone is anisotropic. Abendschein and Hyatt (1970) compared velocity measurements made in bone weakened by disuse osteoporosis to measurements of normal bone. They found that ultrasound velocity and modulus are significantly lower in the bone samples suffering from disuse osteoporosis. Later, this technique was used to measure the nine independent orthotropic elastic coefficients of a single specimen of cortical or trabecular bone (Ashman *et al.* 1984; Ashman, Rho, 1988). The elastic moduli of trabecular bone determined using ultrasound are highly correlated to the moduli

determined by mechanical testing (Ashman *et al.*1987; Ashman *et al.*1989). Although this method is an accurate and nondestructive way to determine modulus, it requires not only ultrasound velocity but also apparent density measurements, and thus cannot be performed in vivo. Another study showed that the yield strength of bovine trabecular bone cubes could be predicted by a combination of density and ultrasound velocity with a coefficient of determination (r^2) of 0.77 (Turner, Eich, 1991).

Researchers have also examined the relationships between ultrasound velocity measurements and skeletal status of bone in vivo. Transmission velocity measurements made in the calcaneus of sheep suffering from disuse osteoporosis were 9.0% lower than measurements made in control animals (Rubin *et al.*1988). Jeffcott and McCartney showed that third metacarpal bone velocity gradually increases in horses between birth and skeletal maturity at 42 months. Also, bone velocity was significantly lower in horses examined with clinical signs of bone problems (i.e., sore shins, bone fracture) (Jeffcott, McCartney, 1985).

Several researchers have investigated the relationship between skeletal status and the apparent velocity of ultrasound (AVU), the velocity of ultrasound measured through the patella in vivo. Heaney *et al* (1989) showed that AVU in postmenopausal women with traumatic vertebral compression deformities was significantly lower than in women with no vertebral deformities. Women with AVU measurements below 1825 m/s were found to be six times more likely to suffer a fracture than women with AVU measurements greater than 1825 m/s. Also, AVU could detect osteoporosis as well as DPA of the lumbar spine (Heaney *et al.*1989).

Recent work continues to suggest that AVU is a good predictor of fracture risk. Two related studies have demonstrated that: 1) AVU can discriminate between subjects with and without a history of low-trauma fractures, and 2) AVU is as good as forearm densitometry as a predictor of fracture risk (Travers-Gustafson *et al.*1994; Stegman *et al.*1994).

Others have also investigated in vivo ultrasound transmission velocity through the femur (Andre *et al.* 1980), radius and ulna (Greenfield *et al.* 1975; Greenfield *et al.* 1981; Wright *et al.* 1987), as well as ultrasound velocity along the length of the tibia (Stuessi, Faeh, 1988). Ultrasound velocity, in one form or another, continues to be a promising tool for predicting bone strength and fracture risk.

Development of Ultrasound Attenuation

In addition to ultrasound velocity, the attenuation of ultrasound is frequently used to characterize skeletal status. Langton *et al* (1984) was the first to propose using the slope of the attenuation versus frequency curve as a measure of bone fragility. They assessed specimens of bovine trabecular bone in vitro as well as human calcaneal specimens in vivo, and showed that BUA measurements are repeatable and dependent on the bone mineral content of the bone. The slope of the attenuation - frequency curve was lower for measurements made on elderly women with hip fractures than for young healthy women.

The relationship between bone density and ultrasound attenuation has been more clearly defined by several other groups. In vitro measurements of human and bovine trabecular bone are correlated to bone density with correlation coefficients (r) ranging from 0.50 to as high as 0.99 (McKelvie *et al.* 1989; McCloskey *et al.* 1990; Evans, Tavakoli, 1990; Tavakoli, Evans, 1991).

These in vitro studies have been followed by many clinical studies examining the relationship between BUA of the calcaneus and bone density. BUA of the calcaneus is moderately correlated to density measurements of the calcaneus, with coefficients of determination (r^2) ranging from 0.31 to 0.53 (Zagzebski *et al.* 1991; Gluer *et al.* 1992; Waud *et al.* 1992; Salamone *et al.* 1994). BUA of the calcaneus is also correlated to density measurements at other sites in the body, including the lumbar spine (r^2 = 0.18 - 0.69), femoral neck (r^2 = 0.17 - 0.76), and distal radius (r^2 = 0.20 - 0.72) (Hosie *et*

al. 1987; Evans *et al.* 1988; Rossman *et al.* 1989; McCloskey *et al.* 1990; Baran, 1991; Salamone *et al.* 1994).

Each of these studies show a significant correlation between calcaneal ultrasound and BMD at various sites in the body. However, the correlations are modest, leading many researchers to speculate that ultrasound is influenced by the structure and morphology of trabecular bone. Thus, the goal of this research was to determine whether ultrasound velocity and attenuation measures of the intact foot are associated with the morphology of calcaneal trabecular bone. Furthermore, we asked whether this association is independent of the density of the trabecular bone.

Chapter 2 - QUS and Trabecular Morphology

Introduction

Quantitative ultrasound (QUS) of the calcaneus has recently been introduced as a technique for assessing skeletal status that may provide advantages to DXA and other conventional techniques. Several investigators have shown that QUS of bone in vitro correlates with bone density (McKelvie *et al.*1989), elastic modulus (Ashman *et al.*1987), and bone strength (Kaufman, Einhorn, 1993). However, ultrasound attenuation and velocity measurements in vivo are only moderately correlated with bone density (Salamone *et al.*1994; Gluer *et al.*1992). Therefore, it has been suggested that ultrasound measurements are influenced by the morphology of trabecular bone, thereby partially explaining the moderate correlation. Ultrasound may provide information about the morphology of trabecular bone that could otherwise only be determined in vitro using either two-dimensional sterology techniques or three-dimensional techniques such as micro-computed tomography (microCT) or micro magnetic resonance imaging (microMRI). However, the ability of QUS to assess trabecular bone morphology in vivo has yet to be determined.

Several researchers have examined the relationship between quantitative measurements of trabecular bone morphology and QUS. Hans *et al* (1993) analyzed the relationship between QUS measurements of the intact cadaveric foot and the two - dimensional architecture of trabecular bone from the calcaneus. They found that ultrasound parameters provided a better indication of the morphology of bone than bone density. Optimized multiple regressions showed that trabecular bone node and terminus numbers, measures of trabecular connectivity, accounted for 80% and 86% of the variation in SOS and BUA, respectively. In another study, Grimm *et al* (1994) found that, in trabecular bone from lumbar vertebrae, average attenuation was inversely correlated to mean trabecular plate spacing, with a coefficient of determination (r^2) of 0.81. Only Hans

et al compared calcaneal ultrasound measurements made in vivo with measures of trabecular morphology, but the morphology parameters were measured in two-dimensional planes.

Recently, Glüer *et al* (Gluer *et al.* 1994) investigated the relationship between trabecular morphology and QUS of bovine trabecular bone. They found weak to moderate correlations between the QUS parameters, trabecular architecture assessed by microCT, and bone mineral density (BMD) assessed by DXA. BMD alone explained 13 and 26% of the variation BUA and AUA, respectively. These correlations increased by 20 to 40% when the trabecular morphology parameters were included. The results were similar for BV. The QUS parameters were significantly correlated with bone morphology independently of bone density. However, these results apply to in vitro measurements made using cubes of bovine bone and thus may not directly provide information about in vivo QUS measurements of trabecular bone.

This project addresses some of the shortcomings of the previous work and asks the following questions: 1) Do QUS measures of human trabecular bone cubes from the calcaneus correlate with trabecular morphology?; 2) Do QUS measures of the calcaneus in intact, human cadaveric feet correlate with the morphology of the trabecular bone in the calcaneus?; and 3) Does QUS provide information about trabecular bone morphology that is independent of bone density?

Materials and Methods

Specimens

Thirty-one pair of cadaveric feet were obtained from the Harvard Medical School Anatomical Gifts Program. The specimens were obtained from 13 male and 18 female donors, with an average age of 77 years, ranging from 50 to 91 years. Sex, age, and cause of death for each donor is listed in Table 1 of Appendix A. Specimens were harvested shortly after death and stored frozen in sealed plastic bags. A radiograph of each

specimen was taken and specimens containing previous fractures, visible metastatic defects, or large osteophytes were excluded.

Quantitative Ultrasound Scanning

Ultrasound analysis of the intact feet was performed using a Walker Sonix UBA 575+ Ultrasound Bone Analyzer (Walker Sonix, Inc., Worchester, MA.) according to the manufacturers' protocol. Feet were completely thawed prior to testing. Immediately prior to scanning, each foot was soaked in soapy water for approximately 5 minutes to ensure adequate skin hydration. We assessed BUA, BV, and SOS. Each foot was scanned twice with repositioning between scans and the average reported. After scanning, the specimens were returned to the freezer. Specific details regarding ultrasound scanning are given in the Beth Israel Hospital Orthopaedic Biomechanics Laboratory Standard Operating Procedure (OBL SOP #IA_U_1) included in Appendix B.

DXA Scanning

Bone density of the calcaneus was estimated using two different methods; dual energy x-ray absorptiometry (DXA) and quantitative computed tomography (CT). DXA scanning was performed on a QDR-2000 x-ray bone densitometer (Hologic, Inc., Waltham, MA). In preparation for DXA scanning, the foot was strapped into a plexiglass bracket so that the angle between the bottom of the foot and the back of the leg was 105°, matching the position of the foot in the ultrasound scanner. Each foot was positioned on the scanning table with the lateral surface facing up. The forearm algorithm was used for

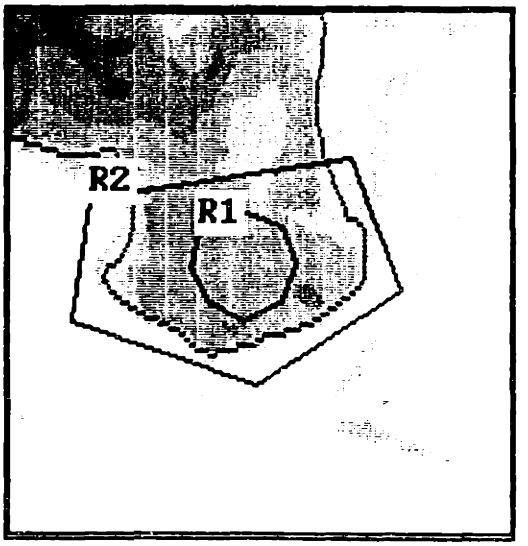

Figure 2-1 Regions of analysis for DXA of the calcaneus

both scanning and analysis (point spacing = 0.0465 cm; resolution = 0.1003 cm). Each foot was scanned twice with repositioning between scans. Details of the DXA scanning procedure are given in Appendix B (OBL SOP #IA_D_10).

We estimated bone mineral density (BMD) from the DXA scans in 2 different regions. BMD of the entire posterior region of the calcaneus was calculated (BMDpost), as well as BMD of circular region (19 mm diameter) within the calcaneus (BMDcirc) (Figure 2-1). The size and location of this circular region was chosen to reproduce the ultrasound transducer characteristics.

CT Scanning

We also estimated bone density using computed tomography (GE 9800, General Electric Medical Systems, Milwaukee, WI). Prior to CT scanning, a steel surgical skin staple was placed on both sides of each foot at the site of the ultrasound scan (Figure 2-2a). The staples were visible on the CT image and served to mark the location of the ultrasound scan on the CT images. Six to ten image slices (3 mm thick) were obtained in the posterior region of the calcaneus and overlapping the skin staples. The scan region included a six chamber, solid hydroxyapatite and polymer phantom which was used to convert CT numbers to equivalent mineral density (Figure 2-2).

The CT scans were analyzed using two different regions to determine bone density. All image viewing and analysis was done using AVS (Advanced Visual Systems, Waltham, MA) image processing software running on a Sun Sparcstation 5. Custom AVS program networks made in the BIH OBL were used for quantitative analysis of the images.

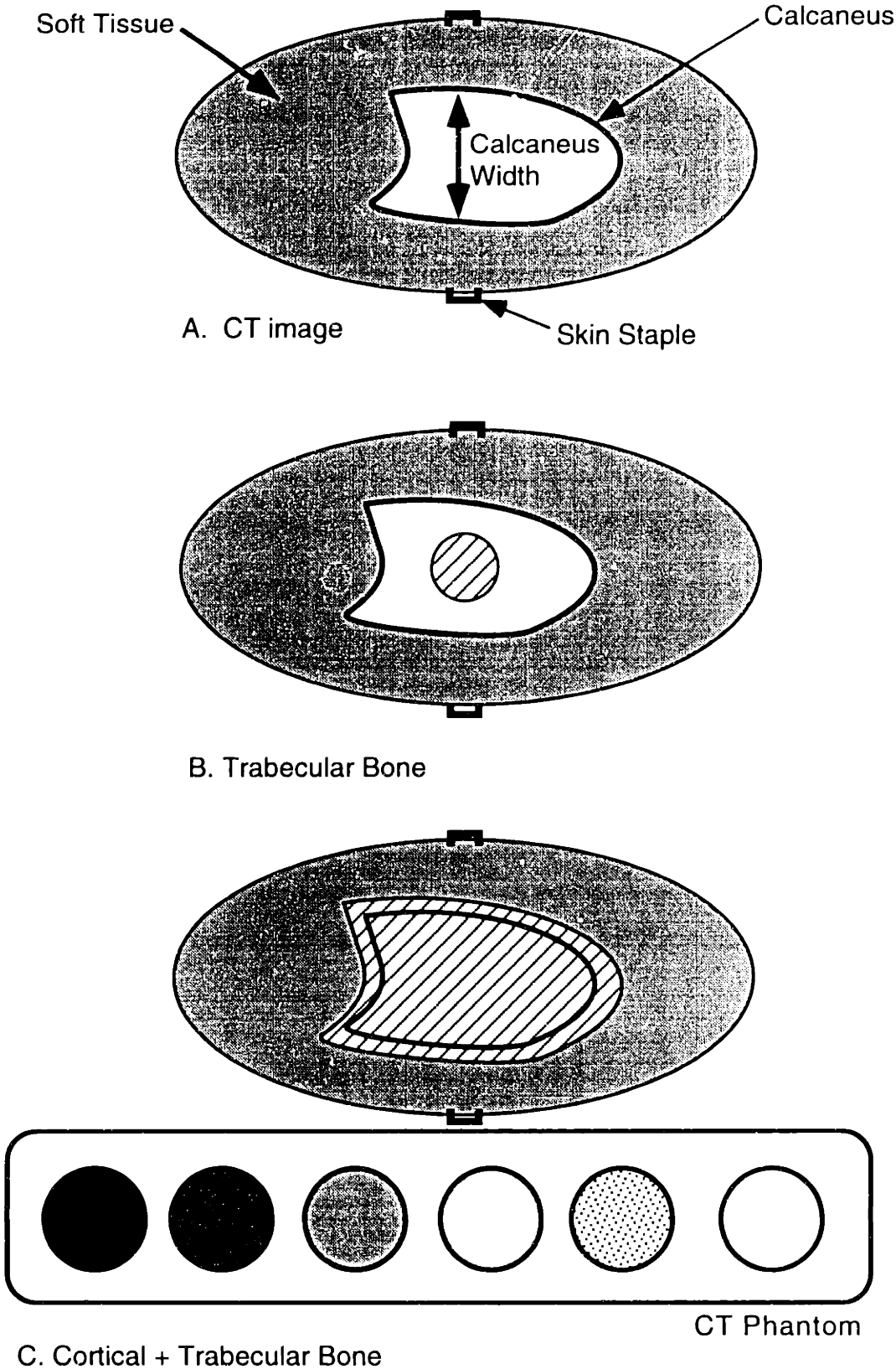

Figure 2-2 Schematic of several CT images of the foot showing the location of the width and density measurements. A. CT image slice showing the calcaneus, skin staples, and soft tissue. B. CT image with 19 mm circular region of interest containing only trabecular bone (BMDcirc). C. CT image with region of interest including the entire calcaneus.

We measured bone density in two different regions of the calcaneus. The first region measured average density of bone in a 19 mm diameter circle positioned in the middle of the calcaneus between the staples (Figure 2-2b). Because of the size and position of the circle, only trabecular bone was included in the measurement.

The average density of the entire slice of the calcaneus was also calculated. The region of interest included both the cortical shell and trabecular bone in the interior of the calcaneus (Figure 2-2c). For each of the different density measurements, the bone density was calculated from three consecutive slices and averaged. OBL SOP #IA_Q_6 and portions of OBL SOP #IA_A_1 (Appendix B) provide the specific procedures for measuring bone density from the CT scans.

Preparation of Trabecular Bone Samples

After density measurements were made, trabecular bone specimens were removed from the calcaneus of one foot from each pair. A cube (15 mm) of trabecular bone was removed from each calcaneus using a Buehler Isomet low speed saw (Buehler Ltd., Lake Bluff, IL) with a diamond tipped blade. The cube was located at the site of QUS scanning and positioned so that the primary trabecular orientation would be in the anterior-posterior direction (Figure 2-3). The exact linear dimensions of each cube were assessed with calipers. A description detailing how the cube was cut from the calcaneus is given in Appendix B.

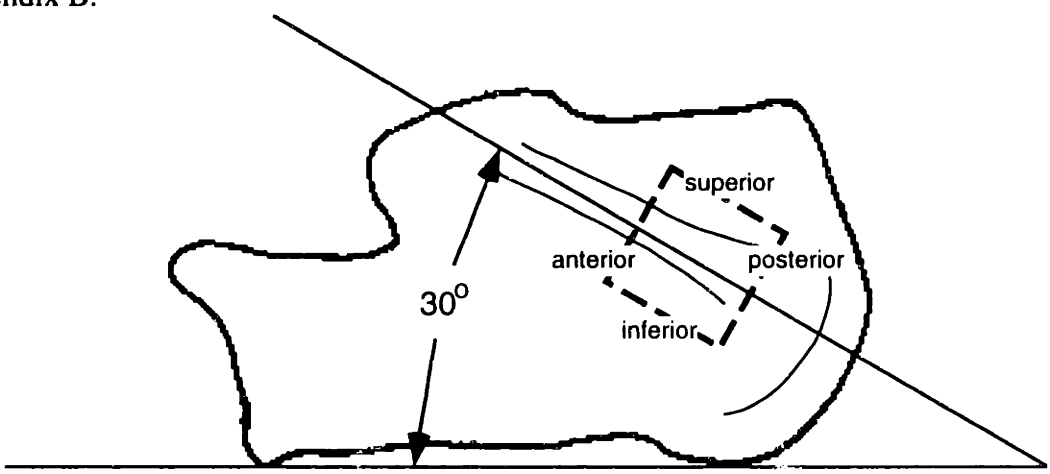

Figure 2-3 Position of the 15 mm trabecular bone cube removed from the calcaneus.

Quantitative Ultrasound of Trabecular Bone Specimens

Next, we scanned each trabecular bone cube using the Walker Sonix UBA 575+. Prior to scanning, each bone specimen was thawed and degassed under vacuum. To perform ultrasound measurements of the cubes, a foam bracket similar to the one used by Glüer *et al* (1993) was used to position the cubes in the scanning device (Figure 2-4).

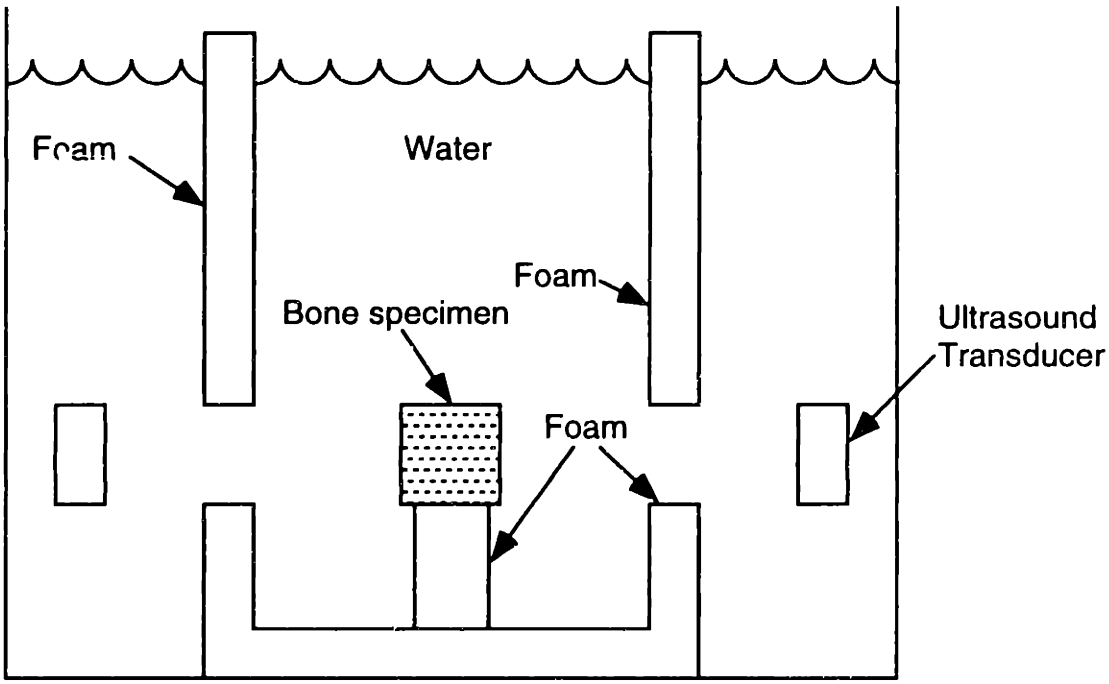

Figure 2-4 Bracket used for QUS scanning of the trabecular bone cubes

QUS measurements were made along the 3 perpendicular axes of the cube: medial-lateral, superior-inferior, and anterior-posterior. We assessed BV, SOS, BUA and average ultrasound attenuation (AUA). AUA was computed as the average attenuation over the frequency range 0.2 to 0.6 MHz. Each specimen was scanned twice in each direction with repositioning between scans and the average reported.

Density Measurements of Trabecular Bone Cubes

BMC and BMD were determined for each trabecular bone specimen using dual energy x-ray absorptiometry (QDR - 2000plus, Hologic, Inc.). The high resolution algorithm was used for scanning and analysis of the cubes. Each cube was scanned once in each of 3 perpendicular directions and the average reported. Density was computed as

the DXA measured bone mineral content divided by the cube volume, as assessed by caliper measurements. A sample output and analysis is shown in Appendix C.

The bone density of each cube was also estimated using peripheral quantitative computed tomography (pQCT) (Stratec XCT 960A, Norland, Inc., Fort Atkinson, WI). Specimens were thawed and degassed in canola oil under vacuum and ultrasonic agitation prior to scanning. Specimens were scanned submerged in canola with: slice thickness = 1.0 mm; slice spacing = 2.0 mm; voxel size = 0.295 mm. Density was calculated for four slices and the mean value used for subsequent analyses.

Trabecular Bone Morphology

Finally, each cube was imaged using microMRI to assess the morphology of the trabecular bone. Before scanning each cube was thawed and degassed in canola oil under vacuum and ultrasonic agitation. The bone remained submerged in the canola oil during microMRI scanning. The cubes were imaged using a 9.7 Tesla Bruker AMX 4000 Wide Bore Spectrometer (Bruker Instruments Inc., Billerica, MA) with a micro imaging attachment. A 32 mm coil was used with a three-dimensional proton spin echo imaging sequence to obtain the images. An 18 mm field of view with 200 data points was used in all directions, resulting in a resolution of 90 m. The acquisition and image reconstruction parameter files as output by the Bruker spectrometer are given in Appendix D.

Morphology parameters were evaluated using a Sun Sparcstation 5, AVS, and specially developed AVS program networks written within the BIH OBL. Prior to morphology analysis, a thresholding routine was applied to each image, creating a binary image where each pixel was assigned to either bone or marrow space. An AVS program network was used to set an optimum threshold level for each image by comparing the edges of the trabecular structure in the original image to the thresholded image. Three - dimensional morphology parameters were calculated from an 11 mm diameter spherical region in the center of the trabecular bone cube.

Table 2-1 lists the morphology parameters that were calculated. The nomenclature recommended by Parfitt *et al* (1987) is used.

Table 2-1 Morphology parameters, units, nomenclature, and formulae

Parameter	units	abbrev.	definition
trabecular volume fraction	mm^3/mm^3	BV/TV	-
trabecular plate number	1/mm	Tb.N	# intersections / test line length
surface to volume ratio of bone	mm^2/mm^3	BS/TV	$2Tb.N/BV/TV$
trabecular plate separation	mm	Tb.Sp	$1 - BV/TV/Tb.N$
trabecular plate thickness	mm	Tb.Th	$BV/TV/Tb.N$
connectivity	$1/mm^3$	Conn.	Euler/vol.
mean intercept length	mm	MIL	$BV/TV/Tb.N$
degree of anisotropy	mm/mm	DA	MIL_1/MIL_3

Trabecular volume fraction (BV/TV) is the ratio of trabecular bone per total bone volume; it is evaluated directly from the image. Saltykov's (1958) method of directed secants was used to evaluate many of the other morphology parameters. The method involves traversing the three - dimensional bone and marrow space with an array of uniformly distributed test lines. For each line, the number of transitions between bone and marrow is determined. This procedure is repeated for 128 random orientations of the test lines. The number of transitions normalized by the test line length is defined here as trabecular number (Tb.N), or intersections / length. The morphology parameters are defined with respect to BV/TV and Tb.N in Table 2-1. The surface to volume ratio (BS/TV) is a measure of the surface area of trabecular bone per volume of trabecular bone. Trabecular plate separation (Tb.Sp) indicates the average distance between trabecular plates, and trabecular plate thickness (Tb.Th) provides a measure of the average thickness of the trabeculae within the specimen.

The method of directed secants was used to calculate the mean intercept length (MIL), a measure of the anisotropy of trabecular bone. MIL is a two - dimensional vector

quantity (i.e. MIL(,)) based on Tb.N and BV/TV (Table 2-1). An ellipse can be fit to the MIL vectors when the vectors are plotted against test line orientation. The ratio of major to minor axes of the ellipse (MIL_1/MIL_3) is a measure of the degree of anisotropy (DA) of the trabecular bone.

Connectivity is given quantitatively by the Euler number, an indication of how well the elements of the bone matrix are connected to each other. The Euler number is only a measure of the number of bone connections; it does not provide information about the shape, position, or strength of the connection. To calculate the Euler number, every pixel within a test region that represents bone is assigned a value of +1. Each junction between pixels representing bone is assigned a value of -1. The Euler number is the sum of the bone pixels (+1) and the connecting pixels (-1) within the test region. Euler number is normalized by volume to provide a measure of connectivity.

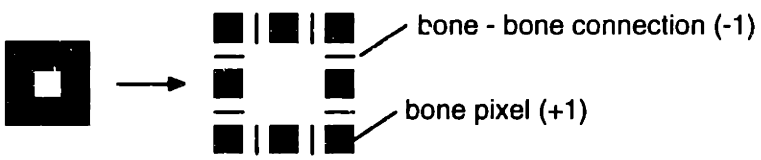

$$\text{Euler conn.} = \sum \text{bone pixels} + \sum \text{pixel connections}$$

$$= 8(+1) + 8(-1) = 0$$

Figure 2-5 Calculation of Euler connectivity

Statistical Analysis

Statistical analysis was performed to evaluate QUS, density, and the morphology parameters. Descriptive statistics were calculated each group of data (Appendix A). To determine the coefficients of determination (r^2) between groups of variables, linear regressions were performed between the density, morphology, and QUS of the trabecular bone cubes, as well as for the morphology and intact foot QUS and density measurements.

Correlations with $p < 0.05$ were considered significant. Finally, multiple linear regressions were performed to determine if density and QUS measurements are independent predictors of morphology. In the multiple regression, the morphology parameters were considered dependent variables. For the trabecular bone specimens density (from pQCT) and QUS were independent variables. Density was added to the regression first, then we tested each QUS parameter to determine if it significantly ($p < 0.10$) reduced the amount of variability in the regression. The process was repeated for density (from DXA) and QUS of the intact feet.

Results

Results are presented for 20 calcaneal trabecular bone specimens, as we were unable to evaluate morphology parameters for the remaining 11 specimens due to poor microMRI image quality.

Since there was no soft tissue surrounding the trabecular bone cubes, BV and SOS measurements were highly correlated ($r = 0.99$, $p < 0.001$). Thus, only SOS values are presented in subsequent analyses. The average QUS parameters are reported, since the density and the morphology parameters are averaged over the entire volume of the cube. In addition, since bone density assessed by DXA and pQCT were very highly correlated ($r = 0.96$, $p < 0.001$), only bone density assessed by pQCT is reported. Data for each specimen, including DXA and pQCT bone density (Table A-3), directional attenuation (Table A-4), directional velocity (Table A-5), and morphology (Table A-6) are given in Appendix A.

The descriptive statistics for the measurements made on the calcaneal trabecular bone cubes and the intact feet are shown in Tables 2-2 and 2-3, respectively.

Table 2-2 Descriptive statistics for calcaneal trabecular bone morphology parameters, cube density, and average QUS measures. (n = 20)

		mean	SD	range
BV/TV	(mm^3/mm^3)	0.33	0.09	0.18 - 0.53
BS/TV	(mm^2/mm^3)	12.13	2.04	7.51 - 16.91
Tb.Th	(mm)	0.17	0.03	0.12 - 0.27
- Conn.	($1/mm^3$)	0.44	0.18	0.10 - 0.73
DA	(mm/mm)	1.30	0.05	1.11 - 1.42
Tb.N	(1/mm)	1.95	0.30	1.35 - 2.35
Tb.Sp	(mm)	0.36	0.11	0.21 - 0.59
Density*	(g/cc)	0.187	0.07	0.03 - 0.30
avg. AUA†	(dB)	15.1	6.6	2.0 - 31.5
avg. BUA	(dB/MHz)	11.8	6.2	2.8 - 21.9
avg. SOS	(m/s)	1486	7	1477 - 1502

*Bone density as assessed by pQCT †Average represents the geometric mean of measurements in the ML, AP, and SI directions.

Only the 19 mm circle CT and BMDcirc density measurements are reported. The regions of analysis for these measurements most closely match the regions of bone analyzed by QUS (Table 2-3).

Table 2-3 Descriptive statistics of calcaneal trabecular bone density and QUS parameters of intact cadaveric feet. (n = 20)

		mean	SD	range
BMDcirc	(gm/cc)	0.49	0.17	0.07 - 0.80
CT 19mm	(gm/cc)	0.15	0.05	0.07 - 0.23
BUA	(dB/MHz)	52.9	20.5	8.0 - 92.5
BV	(m/s)	1659	114	1476 - 1987
SOS	(m/s)	1515	19.8	1480 - 1571

Bone density was moderately to strongly associated with all of the trabecular bone morphology parameters (Table 2-4). Correlations between QUS and morphology yielded several interesting results: 1) Two of the morphology parameters did not correlate to average QUS values, trabecular number (Tb.N) and Euler connectivity, 2) Trabecular spacing (Tb.Sp) was only correlated to BUA, 3) Trabecular thickness (Tb.Th) and BS/BV were strongly correlated to QUS velocity measures, and 4) AUA was not correlated to most of the morphology parameters, and only weakly correlated to BS/TV

and Tb.Th. In general, the morphology parameters were best correlated to the average of the directional QUS measurements. Euler connectivity was an exception, while not significantly correlated to the average QUS measurements, it was weakly correlated to BUA ($r = 0.46$, $p < 0.05$) and SOS ($r = 0.50$, $p < 0.05$) measurements in the SI direction.

Results also showed that cube QUS and bone density were moderately to strongly correlated. Density (from pQCT) was moderately correlated to average AUA and highly correlated to average BUA and SOS. Figures 2-6, 2-7 and 2-8 show some of the correlations between morphology and QUS and density measurements for both the trabecular bone specimens and intact cadaveric feet.

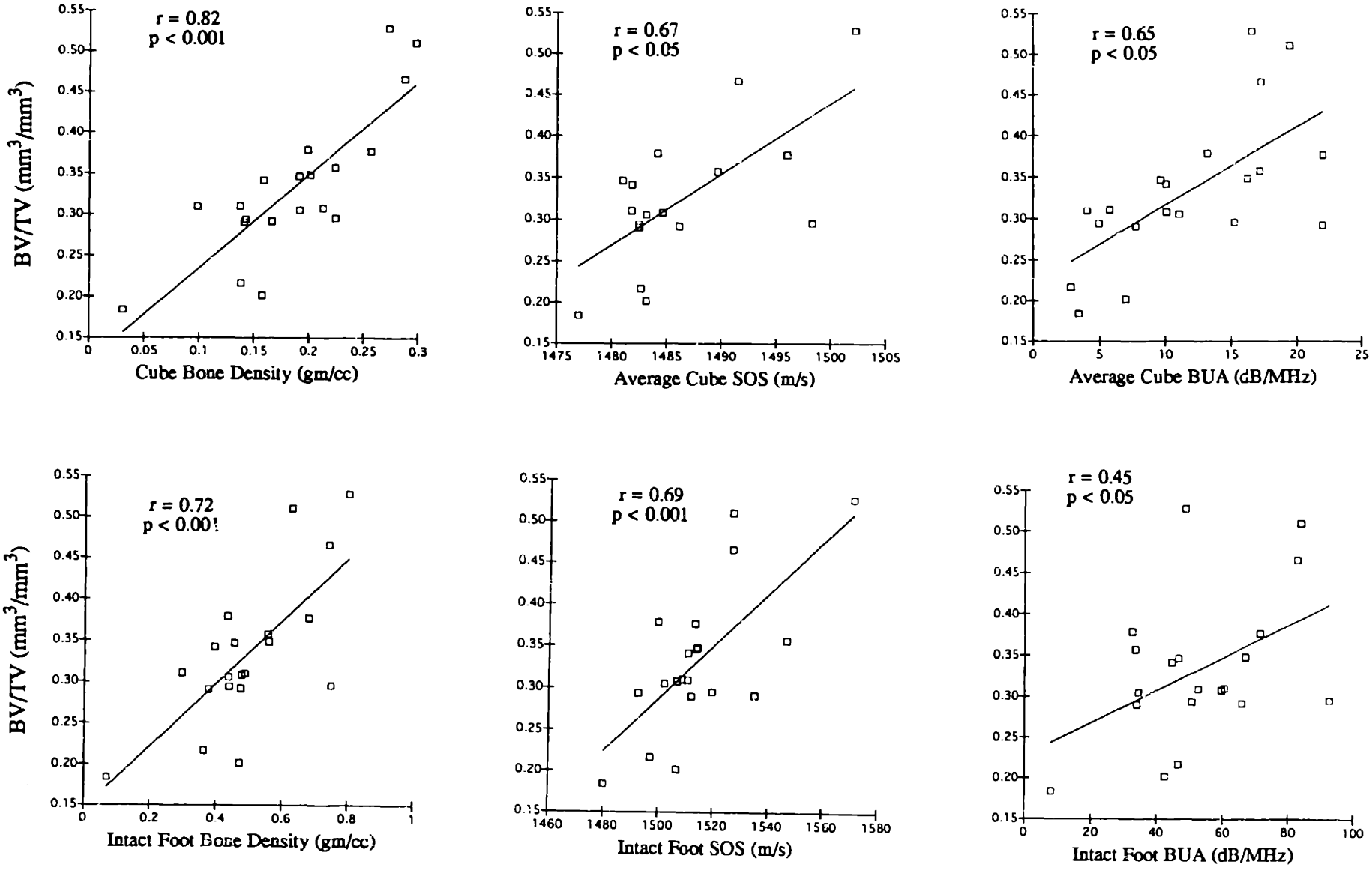

Figure 2-6 Relationships between trabecular volume fraction and density and QUS parameters of trabecular bone specimens (top) and intact cadaveric feet (bottom). (n = 20)

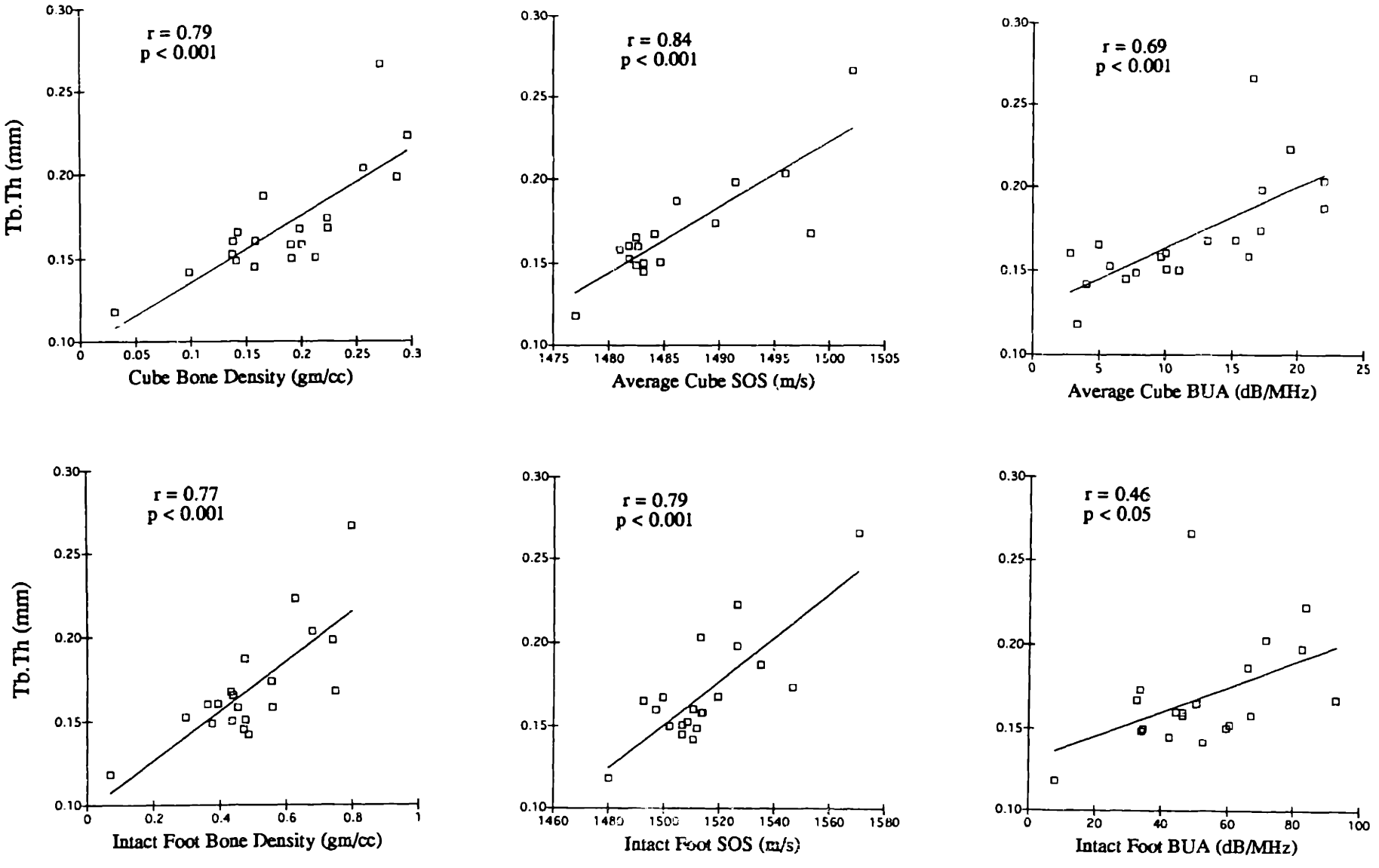

Figure 2-7 Relationships between trabecular thickness and density and QUS parameters of trabecular bone specimens (top) and intact cadaveric feet (bottom). (n = 20)

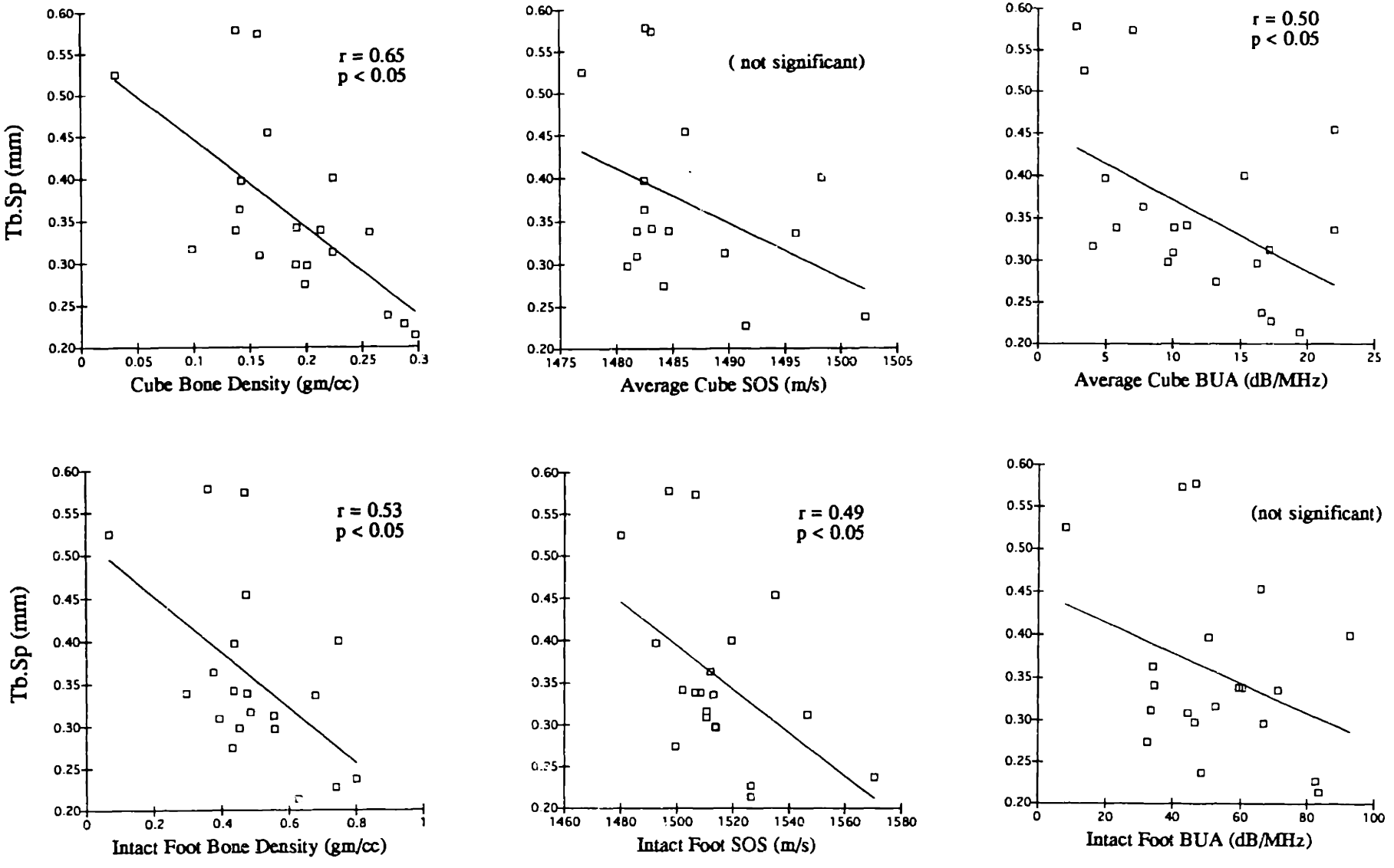

Figure 2-8 Relationships between trabecular spacing and density and QUS parameters of trabecular bone specimens (top) and intact cadaveric feet (bottom). (n = 20)

Table 2-4 Correlation coefficients (r) for morphology, QUS, and density parameters measured in cubes of trabecular bone from the calcaneus. (n = 20) All correlations $p < 0.001$, except $^{+}p < 0.05$

	BV/TV	BS/TV	Tb.Th	Euler conn.	Tb.N	Tb.Sp	DA	pQCTdens	AUA_avg	BUA_avg	SOS_avg
BV/TV	1.00										
BS/TV	-0.84	1.00									
Tb.Th	0.85	-0.97	1.00								
Euler conn.	-0.85	0.66	-0.62^{+}	1.00							
Tb.N	0.71	NS	NS	0.74	1.00						
Tb.Sp	-0.88	0.55^{+}	-0.53^{+}	-0.83	-0.94	1.00					
DA	NS	-0.52^{+}	NS	NS	NS	NS	1.00				
pQCTdens	0.82	-0.86	0.79	0.66^{+}	0.47^{+}	-0.65^{+}	0.68	1.00			
AUA_avg	NS	-0.54^{+}	0.46^{+}	NS	NS	NS	NS	0.57^{+}	1.00		
BUA_avg	0.65^{+}	-0.75	0.69	NS	NS	-0.50^{+}	0.53^{+}	0.79	0.75	1.00	
SOS_avg	0.67^{+}	-0.82	0.84	NS	NS	NS	0.50^{+}	0.80	0.70^{+}	0.72^{+}	1.00

Table 2-5 Correlation coefficients (r) for morphology of trabecular bone cubes, density and QUS measurements of intact cadaveric feet. (n = 20) All correlations $p < 0.001$, except $^{+}p < 0.05$

	BV/TV	BS/TV	Tb.Th	Euler conn.	Tb.N	Tb.Sp	DA	BUA	BV	SOS	BMDcirc	CT 19mm
BV/TV	1.00											
BS/TV	-0.84	1.00										
Tb.Th	0.85	-0.97	1.00									
Euler conn.	-0.85	0.66^{+}	-0.62^{+}	1.00								
Tb.N	0.71	NS	NS	0.74	1.00							
Tb.Sp	-0.88	0.55^{+}	-0.53^{+}	-0.83	-0.94	1.00						
DA	NS	-0.52^{+}	NS	NS	NS	NS	1.00					
BUA	0.45^{+}	-0.58^{+}	0.46^{+}	NS	NS	NS	NS	1.00				
BV	0.71	-0.77	0.80	0.48^{+}	NS	-0.51^{+}	NS	NS	1.00			
SOS	0.69	-0.77	0.79	0.48^{+}	NS	-0.49^{+}	NS	NS	0.99	1.00		
BMDcirc	0.72	-0.82	0.77	0.56^{+}	NS	-0.53^{+}	0.56^{+}	0.71	0.66^{+}	0.72	1.00	
CT 19mm	0.74	-0.77	0.74	0.51^{+}	NS	-0.56^{+}	0.59^{+}	0.74	0.61^{+}	0.64^{+}	0.84	1.00

Anisotropy if the trabecular bone is illustrated by the changes in BUA and SOS with direction (Figure 2-9).

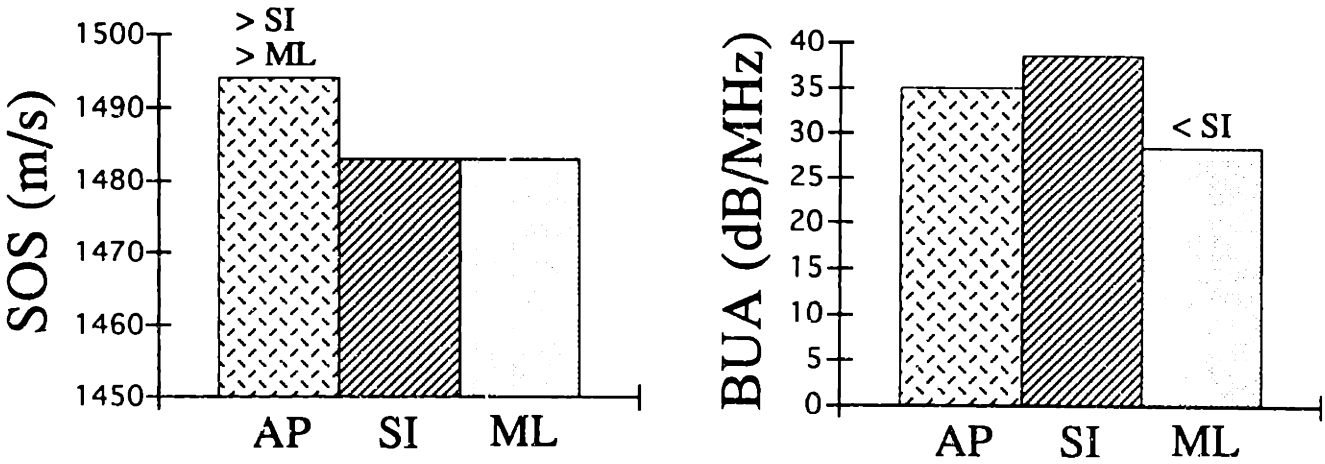

Figure 2-9 Broadband ultrasound attenuation (right) and speed of sound (left) in trabecular bone specimens in the anterior - posterior, superior - inferior, and medial - lateral directions.

Like the trabecular bone cube measurements, with the exception of Tb.N, bone density was moderately to strongly associated with all of the trabecular bone morphology parameters (Table 2-5). The relationships between QUS of the intact foot and morphology parameters were similar to the ones observed for the trabecular bone cubes. Tb.N was not correlated to QUS. Euler connectivity and Tb.Sp were weakly correlated to ultrasound velocity and not significantly correlated to BUA. The ultrasound velocity parameters (BV and SOS) were moderately to highly correlated to BV/TV, BS/TV, and Tb.Th. BV and SOS were in all cases more closely correlated to morphology than BUA.

Multiple linear regressions were performed to determine if quantitative ultrasound provided any information about trabecular bone morphology that was independent of bone density. In four of seven cases, for $p < 0.10$, QUS and density were not independent predictors of morphology. There were, however, some exceptions (Table 2-6).

Table 2-6 Results of stepwise multiple linear regression analysis for density, QUS and morphology measurements of trabecular bone cubes. The morphology parameters were used as the dependent variables. Density (pQCT) and QUS were the independent variables. To determine if density and QUS parameters were independently correlated with morphology, density was added to the regression first, then we tested each QUS parameter to determine if it contributed significantly to the regression. Only the cases where QUS and density are significantly, independently correlated ($p < .10$) are reported.

dependent variable		r^2 or R^2
BV/TV	density	0.68
BS/TV	density	0.73
	density + SOS_avg	0.75
Tb.Th	density	0.62
	density + SOS_ap	0.65
Euler conn.	density	0.43
Tb.N	density	0.22
	density + SOS_ap	0.41
	density + SOS_avg	0.48
Tb.Sp	density	0.41
DA	density	0.46

Table 2-7 Results of multiple linear regression for density (BMDcirc) and QUS of intact cadaveric feet and morphology measurements of trabecular bone cubes. The morphology parameters were used as the dependent variables. Density and QUS were the independent variables. To determine if density and QUS parameters were independently correlated with morphology, density was added to the regression first, then we tested each QUS parameter to determine if it contributed significantly to the regression. Only the cases where QUS and density are significantly, independently correlated ($p < .10$) are reported.

dependent variable		r^2 or R^2
BV/TV	density	0.51
	density + BV	0.61
BS/TV	density	0.67
	density + BV	0.76
Tb.Th	density	0.59
	BV + density	0.74
	SOS + density	0.71
Euler conn.	density	0.31
Tb.N	density	0.11
Tb.Sp	density	0.28
DA	density	0.31

With the exception of Tb.Th, for both the bone cubes and intact feet, density was the best single predictor of morphology. Ultrasound velocity was the single best predictor of Tb.Th.

Discussion

For several years researchers have suggested that QUS of the calcaneus is affected by trabecular morphology, explaining the moderate correlations between QUS and bone density. This study has shown that most trabecular bone morphology parameters are correlated to QUS of bone cubes. BV/TV, BS/TV, Tb.Th, Tb.Sp, and DA were correlated to QUS; Euler connectivity and Tb.N were not correlated. With the exception of Tb.Th, density was better correlated to morphology than QUS. In most cases, a combination of ultrasound and density parameters did not explain the variation of morphology better than density alone. The relationship between QUS, density, and Tb.N

was an exception to this trend. The correlation between Tb.N and pQCT density is low ($r^2 = 0.22$). However, when the average SOS is combined with density, the correlation to Tb.N improves significantly ($R^2 = 0.48$) (Table 2-6).

Similar results were observed for the relationship between QUS and density of the intact foot and trabecular morphology. With the exception of Tb.N and DA, QUS was correlated to trabecular morphology. Again, with the exception of Tb.Th, density measures of the intact foot were better correlated to morphology than QUS. Overall, a combination of QUS and density did not explain the variability in morphology better than density alone. In three cases, however, this was not true. Ultrasound velocity and BMD were independent predictors of BV/TV, BS/TV, and Tb.Th (Table 2-7). An increase of ~0.10 or less in r^2 was observed when velocity was combined with density.

The mean of six out of seven of the morphology parameters were within the range of trabecular morphology values reported by Goulet *et al* (1994) and Feldcamp *et al* (1989). Euler connectivity was lower than the values reported by Goulet *et al* (1994). We attribute the discrepancy to differing assumptions about the structure of trabecular bone that led to different calculation methods for the Euler connectivity.

To date few researchers have compared QUS and trabecular bone morphology. With the exception of an abstract published by Hans *et al* (1993), the relationship between QUS of the intact foot and trabecular bone morphology has not been examined. The results published by Hans *et al* agree with our findings. QUS is correlated to trabecular morphology, but bone mineral density is better correlated to morphology than QUS. However, by using optimized multiple regressions, they showed that a combination of morphology parameters could predict BUA and SOS better than BMD.

In another study using cores of trabecular bone from human lumbar vertebrae, Grimm *et al* (1994) found that BUA was very highly correlated to Tb.Sp. In our study, BUA was the only ultrasound measurement made on a trabecular bone cube that was significantly correlated to Tb.Sp, but the correlation was weak.

Glüer *et al* (1994), using bovine trabecular bone, found that AUA, BUA, and BV were significantly correlated with morphology independent of bone density. Their finding conflicts with ours, which showed that most QUS and density parameters are not independent predictors of morphology. However, their findings are from bovine trabecular bone, and may not be comparable to human bone.

Our research had several limitations that we were not able to fully address. The sample size of 20 was small; greater statistical power could have been achieved with additional bone specimens. However, each specimen originated from a different donor; many studies have included more than one specimen from the same donor, eliminating some of the variability from specimen to specimen.

Cadaveric material was used in this study; our protocol would not have been possible without it. McCloskey *et al* (1990) showed that QUS measurements made on feet before and after amputation were not statistically different, suggesting that cadaveric material does adequately approximate true in vivo results. In addition, the cadaveric specimens were kept frozen when not in use, and efforts were made to minimized freeze - thaw cycles.

Morphology analysis showed that the thinnest trabecular strut in our group of bone specimens was about 120 m thick, only slightly larger than the 90 m resolution we achieved with microMRI imaging. A higher imaging resolution would have been desirable to better define the morphology of the low density specimens.

Finally, no physical measurements of density were made of the trabecular bone cubes. DXA and pQCT may not have provided a totally accurate measurement of bone density, especially for the low density cubes.

Despite these limitations, this study has several advantages over previous research. QUS and morphology measurements were made on the calcaneus and calcaneal trabecular bone. Because clinical measurements of QUS are made at the calcaneus, our findings may be more clinically applicable than ultrasound and morphology measurements of bone taken

from other skeletal sites. After QUS scans of the intact feet were made, the trabecular bone specimens that were used to determine morphology were removed from the calcaneus in the location of the QUS scans. One axis of the cube was aligned in the direction of the QUS scan, another in the direction of the principle trabecular orientation. Thus, we can directly compare QUS measurements of the intact foot to morphology.

Finally, the same ultrasound apparatus was used to make QUS measurements on both the intact feet and the trabecular bone cubes. This eliminates some of the variability between QUS of the cadaveric feet and QUS of the trabecular bone cubes.

The clinical implications of changes in trabecular morphology are not completely understood. Although we have established that QUS measures of the calcaneus in vivo correlate to trabecular morphology, it is not clear what information morphology provides about fracture risk or bone strength at common fractures sites. We have also established that QUS and density are not independent predictors of morphology in most cases, but it is still not known what QUS is actually measuring. Finally, is it necessary or relevant, in the clinical setting, to measure both the QUS parameters and bone mineral density? Both QUS and density correlate similarly to morphology. Therefore, the advantages of QUS indicate that ultrasound may be used in place of DXA or QCT as a useful indicator of bone status, although this suggestion should be verified with prospective studies.

Chapter 3
QUS and Mechanical Properties of Trabecular Bone

Introduction

Quantitative ultrasound (QUS) of the calcaneus has recently been introduced as a technique for assessing skeletal status that may provide advantages to DXA and other conventional techniques (see Chapter 1). Several investigators have shown that QUS of bone in vitro correlates with bone density (McKelvie *et al.* 1989; McCloskey *et al.* 1990; Evans, Tavakoli, 1990) and elastic modulus (Ashman *et al.* 1987; Rice *et al.* 1988). Ultrasound attenuation and velocity measurements in vivo are moderately correlated with bone density (Salamone *et al.* 1994; Gluer *et al.* 1992). Furthermore, bone density is strongly associated with the mechanical properties of trabecular bone (Keaveny, Hayes, 1993). However, the *direct* relationship between QUS measurements of the calcaneus and the mechanical properties of trabecular bone has yet to be determined.

Ultrasound velocity is commonly used to evaluate the mechanical properties of engineering materials (1987), and can also be used to determine the modulus of elasticity of a material (Halliday, Resnick, 1988). These measurements are based on the relationship between ultrasound velocity, density, and elastic modulus in a solid, homogeneous material. The relationship is expressed as:

$$v = \sqrt{E/\rho} \ ,$$

where v = ultrasound velocity, E = elastic modulus, and = density. The modulus of elasticity for both cortical (Ashman *et al.* 1984) and trabecular bone (Ashman *et al.* 1987; Ashman, Rho, 1988; Ashman *et al.* 1989) have been measured using this method. Ultrasound has been used to measure the nine independent orthotropic elastic coefficients of single specimen of cortical or trabecular bone (Ashman *et al.* 1984; Ashman, Rho, 1988). Researchers have also determined that ultrasound velocity and elastic modulus are significantly lower in bone samples suffering from disuse osteoporosis (Abendschein,

Hyatt, 1970). Although this method is an accurate and nondestructive way to determine modulus, it requires not only ultrasound velocity, but also apparent density measurements, and thus cannot be performed in vivo.

There is little additional information describing the relationship between calcaneal QUS and the mechanical properties of trabecular bone. Although ultrasound attenuation is related to density, to our knowledge no research has been conducted investigating the correlation between attenuation and the elastic modulus or ultimate strength of bone. Therefore, we asked the following questions: 1) Do QUS measures of human trabecular bone specimens from the calcaneus correlate with their compressive elastic modulus and ultimate strength?; 2) Do QUS measures of the calcaneus in intact, human cadaveric feet correlate with the elastic modulus and ultimate compressive strength of trabecular bone specimens from the calcaneus?; and 3) Do QUS measures provide information about the mechanical properties of bone that is independent of density?

Materials and Methods

As described in Chapter 2, thirty-one matching pairs of cadaveric feet were obtained from the Harvard Medical School Anatomical Gifts Program. Ultrasound analysis of the intact feet was performed using a Walker Sonix UBA 575+ Ultrasound Bone Analyzer (Walker Sonix, Inc., Worchester, MA.) according to the manufacturers' protocol. Bone density of the calcaneus was estimated using two different methods, dual energy x-ray absorptiometry (DXA) and quantitative computed tomography (CT). After the density measurements were made, a cube (15 mm) of trabecular bone was removed from the calcaneus of one foot from each pair (Figure 2-3). Special care was taken to ensure that the sides opposites faces of the bone cubes were parallel. The exact linear dimensions of each cube was assessed with calipers. A QUS scan was made of each trabecular bone specimen along each of the three perpendicular axes of the cube: medial-lateral (ML), superior-inferior (SI), and anterior-posterior (AP) (Figure 2-3). The ML

direction matches the direction of the QUS scan in the intact foot. Average ultrasound attenuation (AUA), broadband ultrasound attenuation (BUA), speed of sound (SOS), and bone velocity (BV) were measured for each cube. The bone density (in g/cc) of each specimen was estimated using peripheral quantitative computed tomography (pQCT).

Finally, mechanical testing was performed on the bone specimens. Prior to mechanical testing the cubes were removed from the freezer and completely thawed. The modulus of elasticity was first determined for each cube in the SI and AP directions using a non-destructive test sequence. The testing order was randomly assigned for testing in the AP and SI directions. The trabecular bone cubes were placed between two platens and compressed in a servohydralic material testing system (Model 1331, Instron Corp., Canton MA). As recommended by Keaveny *et al* (1994), each cube was subjected to eight cycles of conditioning by compressing the specimen to 0.3% strain using a ramp wave at a strain rate of 0.005 /s. Then, the modulus of the specimen was determined by compressing the cube under strain control to 0.4% strain. Strain was measured using a 25 mm gage length extensometer (Model 3542-025M-015-ST, Interlaken Technology Corp., Eden Prairie, MN) attached to the loading platens immediately above and below the bone cube. Force and displacement data was collected and later converted to stress and strain. The modulus of elasticity was defined as the slope of the stress versus strain curve between 0.3% and 0.4% strain.

After the AP and SI moduli were measured, each cube was compressed to failure in the ML direction. To determine modulus and ultimate compressive strength, the cube was compressed to failure following 8 conditioning cycles at 0.3% strain. The ultimate failure load was defined as the maximum load that the specimen supported, or the load at the point where the slope of the load - deflection curve is zero.

Descriptive statistics were calculated for each variable (Appendix A). To determine the association between QUS and mechanical properties, linear regressions were performed between the density, mechanical, and QUS measurements. Correlations

with $p < 0.05$ were considered significant. Finally, multiple linear regressions were performed to determine whether density and QUS measurements were independent predictors of elastic modulus and ultimate strength. In the multiple regression, the elastic modulus and ultimate strength were considered dependent variables. For the trabecular bone specimens, density (from pQCT) and QUS were independent variables. Density was added to the regression first, then we tested each QUS parameter to determine if it significantly ($p < 0.10$) reduced the amount of variability in the regression. The process was repeated using the data obtained from the intact feet, using density (from DXA) and QUS of the intact feet as independent variables.

Final results are given for 20 calcaneal trabecular bone specimens. We did not perform mechanical testing on the 11 remaining specimens. Poor microMRI image quality did not allow us to evaluate the trabecular morphology of the specimens, and we were unwilling to test the specimens destructively without first attempting to improve the microMRI image quality.

Results

Since there was no soft tissue surrounding the trabecular bone cubes, BV and SOS measurements were highly correlated ($r = 0.99$, $p < 0.001$). Thus, only SOS values are presented in subsequent analyses. In addition, in the trabecular bone specimens bone densities assessed by DXA and pQCT were very highly correlated ($r = 0.96$, $p < 0.001$). Thus only bone density assessed by pQCT is reported. The 19 mm circle CT and BMDcirc density measurements (see Chapter 2) are reported for the intact feet, as these regions most closely match the regions of bone analyzed by QUS. Data for each specimen, including DXA and pQCT bone density (Table A-3), directional attenuation (Table A-4), directional velocity (Table A-5), and cube mechanical properties (Table A-7) are given in Appendix A.

The descriptive statistics for the measurements made on the calcaneal trabecular bone specimens and the intact feet are shown in Tables 3-1 and 3-2, respectively.

Table 3-1 Descriptive statistics for trabecular bone cube mechanical properties, bone density, and average QUS measures. (n = 20)

		mean	SD	range
AP Modulus	(MPa)	307	198	11 - 720
SI Modulus	(MPa)	118	85	8 - 342
ML Modulus	(MPa)	85	72	5 - 278
ML Ult. Strength	(MPa)	1.37	1.0	0.10 - 3.37
Density*	(g/cc)	0.187	0.07	0.03 - 0.30
avg. AUA†	(dB)	15.1	6.6	2.0 - 31.5
avg. BUA	(dB/MHz)	11.8	6.2	2.8 - 21.9
avg. SOS	(m/s)	1486	7	1477 - 1502

*Bone density as assessed by pQCT †Average represents the geometric mean of measurements in the ML, AP, and SI directions.

Table 3-2 Descriptive statistics of calcaneal trabecular bone density and QUS parameters of intact cadaveric feet. (n = 20)

		mean	SD	range
BMDcirc	(gm/cm^2)	0.49	0.17	0.07 - 0.80
CT 19mm	(gm/cc)	0.15	0.05	0.07 - 0.23
BUA	(dB/MHz)	52.9	20.5	8.0 - 92.5
BV	(m/s)	1659	114	1476 - 1987
SOS	(m/s)	1515	19.8	1480 - 1571

Bone density assessed by pQCT was moderately to strongly correlated to the mechanical properties of the trabecular bone, explaining 25 to 64% of the variation in modulus and strength (Table 3-3). Some QUS parameters were correlated to the bone mechanical properties, but others were not. Ultimate strength was moderately to strongly correlated with QUS. The best predictor of ultimate strength was average SOS (r = 0.89). The remaining QUS parameters were also weakly to highly correlated to ultimate strength. The correlations between modulus and QUS were lower than those for ultimate strength (Figures 3-2 and 3-2). The best predictor of modulus was BUA (r = 0.73), for measurements in the ML direction. Of the three QUS measures, AUA was the worst predictor of modulus. Only AUA in the SI direction could predict modulus with a weak

to moderate correlation. Elastic modulus, like ultrasound velocity and atttenuation, was significantly higher in the AP direction than in the SI or ML directions (Figure 3-1).

Figure 3-1 Compressive elastic modulus of trabecular bone specimens in the superior - inferior, medial - laterial, and anterior - posterior directions. The modulus in the AP direction is significantly higher than the SI and ML moduli. (n = 20)

The correlations between ultrasound velocity and modulus could be improved by applying the equation relating the parameters together: $v^2 = E$. The product of velocity squared and density was moderately to highly correlated to modulus. However, these correlations were still no better than the correlations between modulus and density alone.

Table 3-3 Correlation coefficients (r) for directional ultrasound parameters and compressive modulus of elasticity (E) for trabecular bone specimens (n = 20) All correlations $p < 0.001$, except $^{+}p < 0.05$

	E_ap	E_si	E_ml	E_avg	ULT_ml	Density*
AUA_ap	NS	NS	NS	NS	0.52^{+}	0.47^{+}
AUA_si	0.46^{+}	0.50^{+}	NS	0.57^{+}	0.69	0.72
AUA_ml	NS	NS	NS	NS	0.57^{+}	0.46^{+}
AUA_avg	NS	NS	NS	NS	0.62^{+}	0.57^{+}
BUA_ap	NS	0.61^{+}	NS	NS	0.52^{+}	0.69
BUA_si	NS	0.73	0.58^{+}	0.62^{+}	0.77	0.84
BUA_ml	NS	NS	0.73	NS	0.57^{+}	0.51^{+}
BUA_avg	NS	0.63^{+}	0.61^{+}	0.54^{+}	0.70	0.79
SOS_ap	NS	NS	0.50^{+}	NS	0.78	0.58^{+}
SOS_si	0.46^{+}	0.75	0.52^{+}	0.66^{+}	0.69	0.82
SOS_ml	NS	0.60^{+}	0.62^{+}	0.57^{+}	0.79	0.70
SOS_avg	NS	0.71^{+}	0.71^{+}	0.58^{+}	0.89	0.81
$(SOS\_ap)^2$	0.61^{+}	0.82	0.62^{+}	0.79	0.79	1.00
$(SOS\_si)^2$	0.56^{+}	0.83	0.70	0.79	0.80	1.00
$(SOS\_ml)^2$	0.56^{+}	0.84	0.71	0.80	0.81	1.00
$(SOS\_avg)^2$	0.62^{+}	0.84	0.62^{+}	0.79	0.78	1.00
Density*	0.55^{+}	0.83	0.70	0.80	0.80	1.00

*Bone density (ρ) as assessed by pQCT.

Similar to the trabecular bone measurements, bone density of the intact foot was also moderately to strongly correlated to the mechanical properties of calcaneal trabecular bone (Table 3-5, Figure 3-3). Ultimate strength was moderately to highly correlated to QUS (Figure 3-4a). Like the trabecular bone cubes, SOS was the best predictor of strength ($r = 0.77$) (Figure 3-4b). BUA and modulus in the ML direction were highly correlated, but the remaining QUS and modulus parameters were either weakly or not at all correlated.

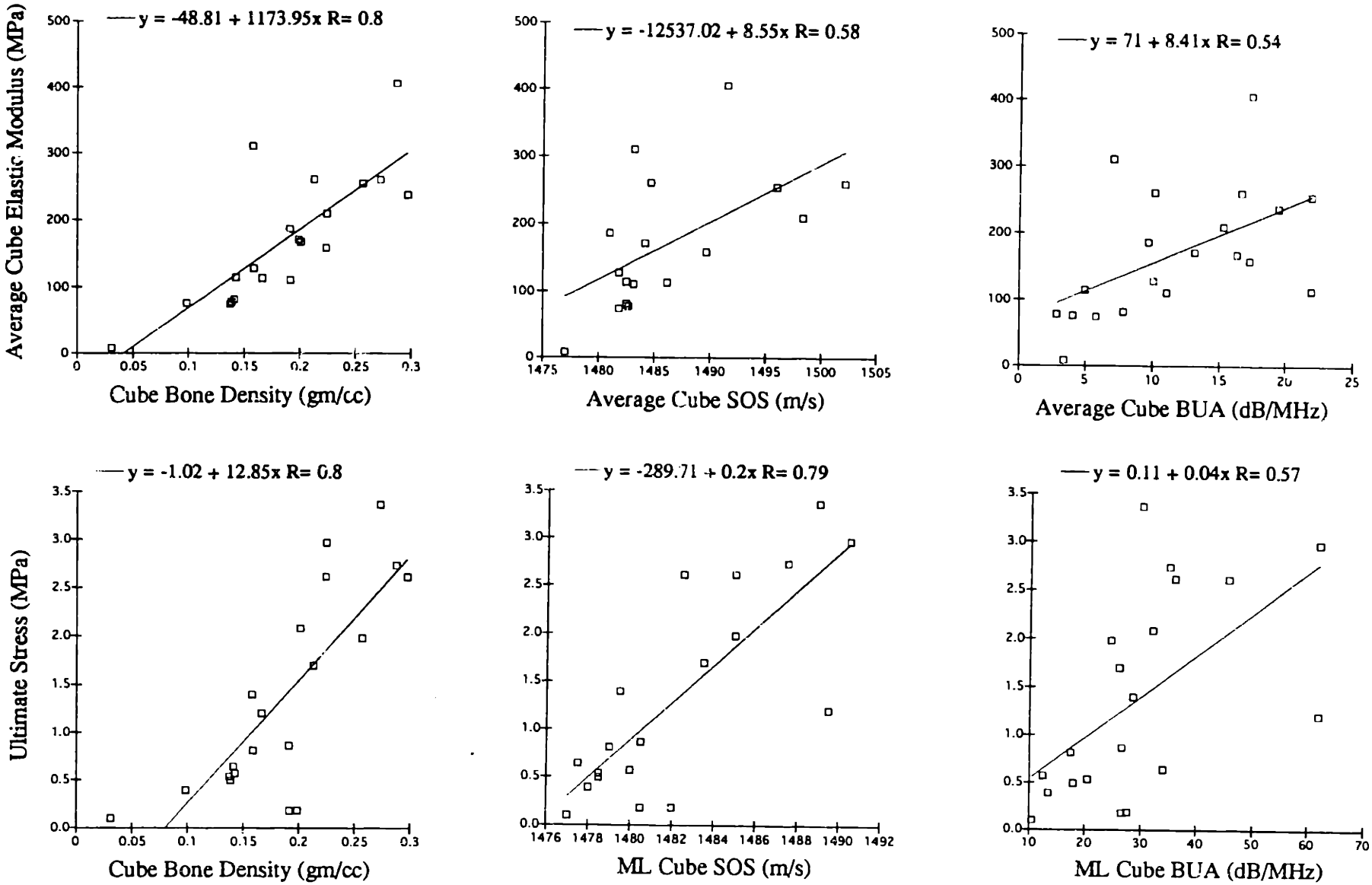

Figure 3-2 Relationships between the mechanical properties of trabecular bone specimens and density and QUS of the specimens. (n = 20, $p < 0.001$, except average cube SOS and BUA, and ML cube BUA, where $p < 0.05$)

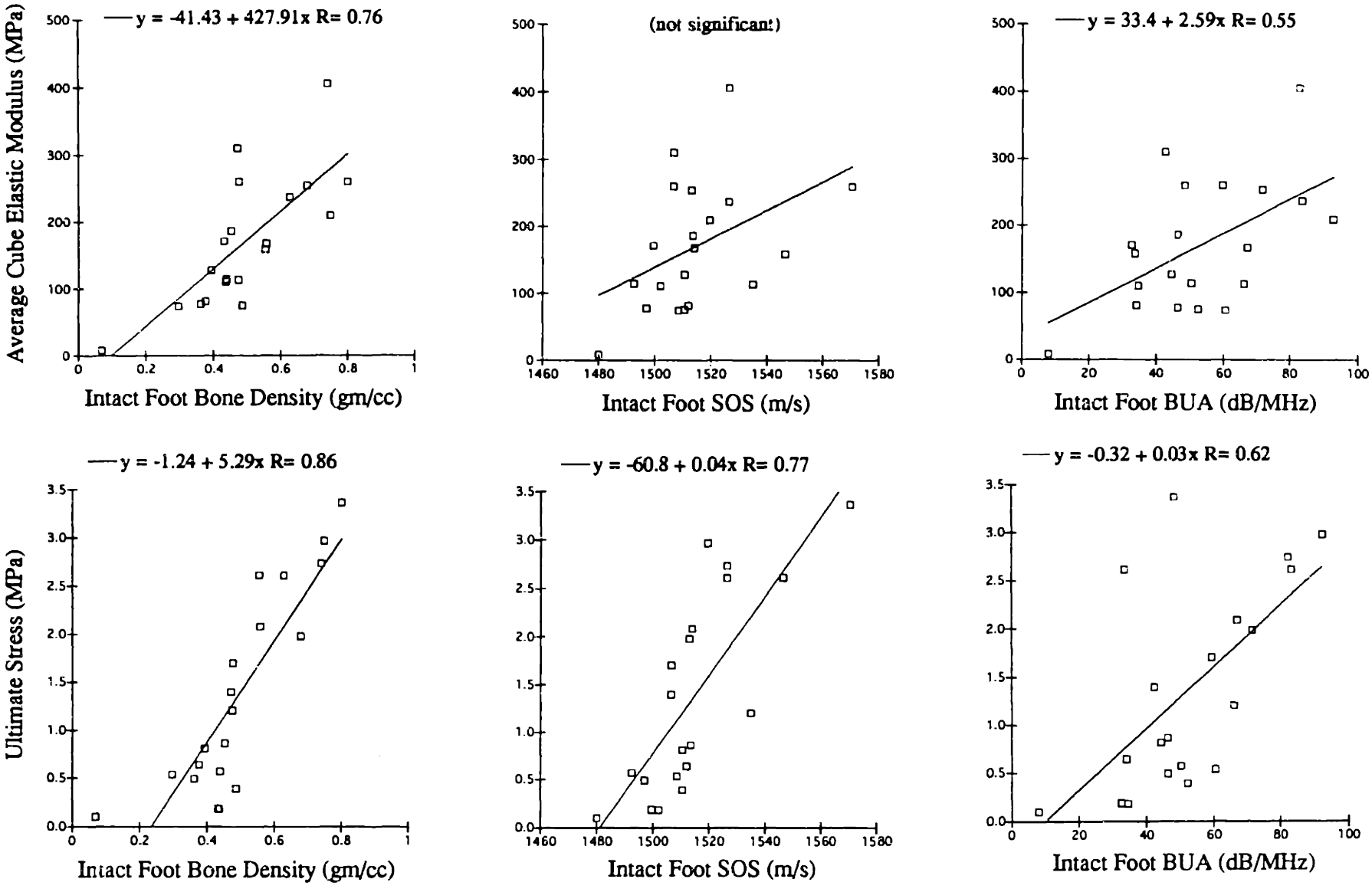

Figure 3-3 Relationships between mechanical properties of calcaneal trabecular bone specimens and density and QUS of intact cadaveric feet. ($n = 20$, $p < 0.001$, except BUA, where $p < 0.05$)

Table 3-5 Correlation coefficients (r) for QUS and density measured in intact cadaveric feet and mechanical properties of calcaneal trabecular bone specimens. (n = 20) All correlations $p < 0.001$, except $^{+}p < 0.05$

	ULT_ml	E_ap	E_si	E_ml	E_avg	BMDcirc	BUA	BV	SOS
ULT_ml	1.00								
E_ap	0.48^{+}	1.00							
E_si	0.70	0.55^{+}	1.00						
E_ml	0.73	NS	0.54^{+}	1.00					
E_avg	0.71	0.91	0.80	0.58^{+}	1.00				
BMDcirc	0.86	0.53^{+}	0.79	0.67^{+}	0.76	1.00			
BUA	0.62^{+}	NS	0.46^{+}	0.71	0.55^{+}	0.71	1.00		
BV	0.74	NS	0.48^{+}	0.45^{+}	NS	0.66^{+}	NS	1.00	
SOS	0.77	NS	0.54^{+}	0.46^{+}	NS	0.72	NS	0.99	1.00

Multiple linear regressions were performed to determine if quantitative ultrasound provided any information about the mechanical properties of bone that was independent of bone density (Tables 3-6 and 3-7). In the trabecular bone cubes, for three of the five variables, density and QUS were independent predictors of mechanical properties. BUA_ml and density were independent predictors of both E_si and E_ml, while SOS and density were independent predictors of ultimate strength.

Multiple linear regressions comparing QUS and density of the intact feet with trabecular bone mechanical properties showed that only SOS and density were independent predictors of ultimate strength (Table 3-7). The same was true for SOS, density, and ultimate strength of the trabecular bone cubes. Density of the intact feet was the best predictor of modulus, adding QUS measurements of the intact feet did not significantly reduce the variability in the regression.

Table 3-6 Results of stepwise multiple linear regression analysis for density (pQCT), QUS, and mechanical properties of calcaneal trabecular bone.

dependent variable		r^2 or R^2
E_ap	density	0.30
E_si	density	0.69
	density + BUA_ml	0.74
E_ml	density	0.49
	density + BUA_ml	0.68
E_avg	density	0.63
ULT_ml	density	0.64
	density + SOS_ml	0.73
	density + SOS_ap	0.76

Table 3-7 Results of stepwise linear regression analysis for density (BMDcirc) and QUS of intact cadaveric feet and mechanical properties of calcaneal trabecular bone.

dependent variable		r^2 or R^2
E_ap	density	0.28
E_si	density	0.62
E_ml	density	0.45
E_avg	density	0.57
ULT_ml	density	0.73
	density + SOS	0.78

Discussion

In this study we asked if QUS measures of intact cadaveric feet and trabecular bone specimens from the calcaneus correlated with the elastic modulus and ultimate strength of the trabecular bone specimens. If so, does QUS provide any information about the mechanical properties of bone that is independent of density? We found that quantitative ultrasound of both trabecular bone specimens and intact cadaveric feet are correlated to the mechanical properties of calcaneal trabecular bone. The was especially true for the ultimate strength of trabecular bone, which was moderately to highly correlated to QUS. In most cases, a combination of ultrasound and density did not explain variations in the mechanical properties better than density alone. However, in 4 out of 10 cases, ultrasound and density were independent predictors of mechanical properties. In these cases, the increase in the coefficient of determination when density and QUS parameters were combined, although statistically significant, was not large enough to be of clinical relevance.

This study has several advantages over previous research. QUS and mechanical properties were evaluated using the calcaneus and calcaneal trabecular bone. Because clinical measurements of QUS are made at the calcaneus, our findings may be more clinically applicable than ultrasound and strength or modulus measurements made using

bone taken from other skeletal sites. After QUS scans of the intact feet were performed, the trabecular bone specimens that were used to determine mechanical properties were removed from the calcaneus in the location of the QUS scans. One axis of the cube was aligned in the direction of the QUS scan, another in the direction of the principal trabecular orientation. Thus, we can directly compare QUS measurements of the intact foot to the mechanical properties of the bone.

Finally, the same ultrasound apparatus was used to make QUS measurements on both the intact feet and the trabecular bone. This eliminates some of the variability between QUS of the cadaveric feet and QUS of the trabecular bone specimens.

The study had several limitations that may have played a role in the experimental outcome. After examining the stress versus strain curves in the ML direction, where the specimens were compressed to failure, it is evident that some of the curves exhibit a large, nonlinear toe region at low levels of strain. This type of stress - strain behavior is typical for biological materials containing collagen. Since the elastic modulus was defined as the slope of the stress vs. strain curve between 0.3% and 0.4% strain, modulus may not have been calculated in the most linear portion of the curve for some specimens. In the AP and SI directions the specimens were only compressed to 0.4% strain, so the modulus cannot be recalculated over a higher range of strain values.

The modulus and ultimate strength data determined using mechanical testing are also highly dependent on specimen geometry. When testing cubes, optimal results are achieved when the opposite sides of the cube are parallel. The sides of some of our cubes may not have been parallel. This is especially true of the low density cubes, where it was difficult to position the cube in the saw without damaging it. However, we exercised caution when cutting the bone cubes to minimize this potential problem.

Although the effects of variation in specimen geometry are reduced by testing many specimens, our sample size of 20 was small. Greater statistical power could have been achieved with additional bone specimens. However, each specimen originated from a

different donor; many studies have included more than one specimen from the same donor, eliminating some of the variability from specimen to specimen.

Finally, the specimens used in this study were obtained from cadaveric material. Our protocol would not have been possible without it. McCloskey *et al* (1990) showed that QUS measurements made on feet before and after amputation were not statistically different, suggesting that cadaveric material does adequately approximate in vivo measurements. In addition, the cadaveric specimens were kept frozen when not in use, and efforts were made to minimized freeze - thaw cycles. Lin *et al* (1993) recently demonstrated that freezing does not effect ultrasound velocity and attenuation measurements in human bone.

The values of modulus and ultimate strength that we measured are similar to reported values (Goulet *et al.*1994; Linde *et al.*1992), although they are on the low end of the reported range. However, since the bone density of many of our specimens was low, smaller values of elastic modulus and ultimate strength are not unusual. Also, specimen geometry and end effects can significantly effect the accuracy of mechanical testing (Keaveny, Hayes, 1993), making it difficult to draw comparisons between different studies.

Contrary to the reports of several authors (Keaveny, Hayes, 1993), our results did not show a strong correlation between compressive strength and modulus. Ultimate strength and modulus in the ML direction were significantly correlated ($r^2 = 0.53$, $p < 0.001$), but not to the degree we expected. The strength - modulus relationships reported in the literature apply to mechanical tests done in the direction of primary trabecular orientation. We tested our specimens to failure in a direction where there was no trabecular orientation, something that may account for the discrepancy.

We have determined that QUS predicts the mechanical properties of trabecular bone in the calcaneus. However, it is not completely clear how well strength of calcaneal trabecular bone predicts bone strength and fracture risk at other sites. The femoral neck,

distal forearm, and lumbar spine are the most common sites of fracture, while calcaneal fractures are relatively uncommon (Melton, 1988). The calcaneus is well suited for QUS measurements because it is comprised primarily of trabecular bone with a thin shell of cortical bone. The presence of trabecular bone is important because the reduction of bone mass observed with osteoporosis is evident first in trabecular bone. Since bone density of the calcaneus can predict incidence of fracture as well as bone density measurements at other sites (Wasnich *et al.* 1987), the high correlation between density and ultimate strength suggests that the ultimate strength of calcaneal trabecular bone may also be a good predictor of bone strength at other skeletal sites. Thus, QUS of the calcaneus may also predict bone status at other sites.

Our data suggests that QUS of the calcaneus may be little more than a different way to measure bone density. Although the precision of QUS is lower than that of DXA and many other x-ray bone density measurement techniques (Hagiwara *et al.* 1994), QUS works as well as density as an indicator of skeletal status. Thus, given that QUS is low cost, easy to use, and radiation free, it could become a useful tool as an indicator of skeletal status.

Chapter 4 - Conclusions and Future Work

For several years researchers have suggested that QUS of the calcaneus is affected by trabecular morphology, thereby explaining the moderate correlations between QUS and bone density. This study has shown that most trabecular bone morphology parameters are correlated to QUS of trabecular bone specimens. However, with the exception of trabecular thickness, density was better correlated to morphology than broadband ultrasound attenuation and speed of sound. In most cases, a combination of ultrasound and density parameters did not explain the variation of morphology better than density alone.

Similar results were observed for the relationship between QUS and density of the intact foot and trabecular morphology. With the exception of trabecular number and degree of anisotropy, QUS was correlated to trabecular morphology. Again, with the exception of trabecular thickness, density measures of the intact foot were better correlated to morphology than QUS. Overall, a combination of QUS and density did not explain the variability in morphology better than density alone.

This study has also shown that quantitative ultrasound of both trabecular bone specimens and intact cadaveric feet are correlated to the mechanical properties of calcaneal trabecular bone. The was especially true for the ultimate strength of trabecular bone, which was moderately to highly correlated to QUS. In most cases, a combination of ultrasound and density did not explain variations in the mechanical properties better than density alone. In the cases where density and QUS were independent predictors of the mechanical properties, the decrease in the amount of unexplained variability, although statistically significant, was not large enough to be of any clinical relevance.

Our data suggests that QUS of the calcaneus may be little more than a different way to measure bone density. Density was usually the best predictor of trabecular morphology or mechanical properties, occasionally QUS was the best predictor. The

combination of QUS and density parameters did not improve these predictions by clinically significant levels. Although the precision of QUS is lower than that of DXA and many other x-ray bone density measurement techniques (Hagiwara *et al.* 1994), this project has shown that QUS works nearly as well as density as an indicator of skeletal status. Thus, given that QUS is low cost, easy to use, and radiation free, it could become a useful tool as an indicator of bone status.

There are several natural extensions of this study that were not addresses in this work. First, we were unable to evaluate the morphology parameters of one third of the trabecular bone specimens because of poor image quality. Future work should investigate why the microMRI image quality was poor, and develop a method to image trabecular bone with a greater level of success.

Furthermore, it is imperative to determine whether combinations of ultrasound parameters predict trabecular bone morphology or mechanical behavior as well as density does. The low correlations between velocity and attenuation suggest that they might be independent predictors of density.

Finally, the data here could be used to determine the relationships between the morphology and the mechanical properties of trabecular bone. This is a broad topic that is beyond the scope of this project, but is one that will have to be addressed to more completely understand the mechanical behavior trabecular bone. The ultimate test of the utility of QUS will be a prospective trial examining fracture risk.

Appendix A - Data

Table A-1

Cadaveric Specimen Data

	specimen ID	sex	age	cause of death	cube side
1	1152	M	75	chronic obstructive pulmonary disease	L
2	1181	M	76	pneumonia	R
3	1189	F	83	intractable pulmonary edema, aortic stenosis	R
4	1194	M	73	ASHD	R
5	1197	M	74	Laënnec's cirrhosis	L
6	1199	M	81	acute MI	L
7	1203	M	73	CHF	R
8	1215	F	50	disseminated CA (breast/ovary?)	L
9	1240	F	74	cardio-pulmonary arrest	L
10	1260	F	82	cardio-pulmonary arrest	L
11	1277	M	81	cardiac arrest	L
12	1282	M	77	myelodysplastic syndrome	R
13	1293	F	89	MI	R
14	1298	F	82	ASHD	R
15	1306	F	85	respiratory failure	L
16	1309	F	78	coronary artery disease	R
17	1317	F	78	septicemia, bladder CA	R
18	1323	F	88	cardio-pulmonary arrest	R
19	1328	F	88	sepsis	R
20	1337	M	79	Parkinson's disease	L
21	1376	F	91	renal failure	R
22	1378	F	84	acute respiratory failure	L
23	1386	F	83	cardiogenic shock	L
24	1399	F	64	lung Hodgkin's lymphoma	R
25	1407	F	86	CHF	L
26	1412	F	85	CHF, ASHD	R
27	1420	M	76	cardio-pulmonary arrest	L
28	1422	F	91	cardio-pulmonary arrest	L
29	1429	M	91	colon CA	R
30	1460	M	78	generalized arteriosclerosis	R
31	1465	M	72	arteriosclerosis	L

MI - myocardial infarction
CA - cancer
CHF - congestive heart failure
ASHD - arteriosclerotic heart disease

- 13 M, 18 F subjects, average age 79.6 years, range = 50 - 91
- 15 left, 16 right side cubes

Table A-2

Intact Feet QUS and Density

specimen ID	fBUA (dB/MHz)	fBV (m/s)	fSOS (m/s)	BMDcirc (gm/cm^2)	BMDpost (gm/cm^2)	CT 19mm (gm/cc)	CT whole (gm/cc)
1152L	42.5	1596.5	1506.5	0.472	0.596	0.1334	0.1937
1181R	33.5	1834	1546.5	0.556	0.608	0.1643	0.2038
1189R	66	1779	1535	0.475	0.578	0.136	0.2122
1194R	50.5	1531.5	1492.5	0.439	0.533	0.0962	0.2053
1197L	52.5	1610	1510.5	0.487	0.468	0.0874	0.1371
1203R	48.5	1986.5	1570.5	0.801	0.83	0.2063	0.2920
1293R	60.5	1638	1508.5	0.297	0.417	0.1629	0.1869
1298R	46.5	1674	1513.5	0.454	0.507	0.1204	0.1864
1309R	59.5	1626	1506.5	0.477	0.514	0.1564	0.2085
1317R	34.5	1600.5	1502	0.437	0.514	0.1244	0.1917
1328R	46.5	1550	1497	0.363	0.436	0.0957	0.1586
1337L	82.5	1684.5	1526.5	0.741	0.768	0.2304	0.2844
1378L	32.5	1570.5	1499.5	0.433	0.5	0.1364	0.1955
1386L	83.5	1761	1526.5	0.629	0.626	0.2167	0.2285
1407L	34	1655	1512	0.377	0.345	0.1154	0.1248
1412R	8	1476	1480	0.069	0.118	0.0655	0.1092
1422L	44.5	1636	1510.5	0.394	0.454	0.1108	0.1825
1429R	67	1655.5	1514	0.559	0.659	0.1626	0.2325
1460R	92.5	1662	1519.5	0.749	0.773	0.2034	0.2579
1465L	71.5	1652	1513	0.68	0.711	0.2112	0.2415
mean	52.85	1659	1514.5	0.4945	0.5478	0.1468	0.2017
sd	20.5	113.5	19.82	0.171	0.163	0.0475	0.0476
min	8	1476	1480	0.069	0.118	0.0655	0.1092
max	92.5	1986.5	1570.5	0.801	0.83	0.2304	0.292

Table A-3

Cube QUS and Density

specimen ID	AUA_AVG (dB)	BUA_AVG (dB/MHz)	SOS_AVG (m/s)	BV_AVG (m/s)	pQCTdens (gm/cc)	DXAdens (gm/cc)
1152L	14.25	7.00	1483.2	1490.5	0.1579	0.0959
1181R	16.38	17.22	1489.7	1524.7	0.2238	0.1672
1189R	27.35	21.94	1486.2	1509.7	0.1664	0.1449
1194R	10.75	4.94	1482.5	1485.2	0.1425	0.0632
1197L	9.14	4.06			0.0983	0.0317
1203R	20.90	16.61	1502.2	1598.0	0.2728	0.2270
1293R	8.76	5.78	1481.8	1481.5	0.1374	0.0788
1298R	12.07	9.67	1481.0	1478.7	0.1912	0.1313
1309R	17.60	10.11	1484.7	1496.5	0.2129	0.1689
1317R	12.73	11.06	1483.2	1490.7	0.1918	0.1468
1328R	10.00	2.83	1482.7	1486.5	0.1385	0.0736
1337L	16.12	17.33	1491.5	1534.5	0.2874	0.2386
1378L	13.80	13.17	1484.2	1494.0	0.1989	0.1487
1386L	14.91	19.44			0.2972	0.2427
1407L	11.86	7.78	1482.5	1488.0	0.1410	0.0696
1412R	1.97	3.39	1477.0	1460.8	0.0310	0.0156
1422L	12.10	10.06	1481.8	1484.2	0.1588	0.0837
1429R	31.53	16.28			0.2011	0.1429
1460R	20.58	15.28	1498.3	1576.0	0.2245	0.1903
1465L	18.65	21.94	1496.0	1552.2	0.2569	0.1632
mean	15.07	11.79	1486.4	1507.7	0.1865	0.1312
sd	6.63	6.18	6.86	37.36	0.066	0.066
min	1.97	2.83	1477.0	1460.8	0.0310	0.0156
max	31.53	21.94	1502.2	1598.0	0.2972	0.2427

Table A-4

Cube Directional Ultrasound Attenuation

	AUA_ML (dB)	**AUA_SI** (dB)	**AUA_AP** (dB)	**BUA_ML** (dB/MHz)	**BUA_SI** (dB/MHz)	**BUA_AP** (dB/MHz)
1152L	13.6	14.3	14.9	28.5	22.0	12.5
1181R	13.5	19.1	16.6	36.0	66.0	53.0
1189R	28.6	25.4	28.1	62.0	64.5	71.0
1194R	5.2	11.8	15.2	12.5	18.0	14.0
1197L	4.6	7.1	15.8	13.5	19.5	3.5
1203R	19.0	21.4	22.3	30.0	66.5	53.0
1293R	6.6	8.1	11.6	20.5	21.0	10.5
1298R	9.9	11.1	15.1	26.5	26.5	34.0
1309R	12.8	19.8	20.2	26.0	45.0	20.0
1317R	9.0	13.9	15.3	26.5	41.0	32.0
1328R	8.7	9.8	11.5	18.0	5.0	2.5
1337L	12.6	19.1	16.7	35.0	69.0	52.0
1378L	10.9	16.9	13.6	27.5	40.0	51.0
1386L	12.9	17.6	14.3	45.5	70.0	59.5
1407L	11.3	10.5	13.7	34.0	19.5	16.5
1412R	1.0	1.6	3.3	10.5	10.0	10.0
1422L	6.6	12.6	17.2	17.5	30.0	43.0
1429R	32.0	29.2	33.3	32.0	61.0	53.5
1460R	20.5	19.7	21.6	62.0	51.5	24.0
1465L	12.4	22.6	21.0	24.5	84.5	88.5
mean	12.6	15.6	17.1	29.4	41.5	35.2
sd	7.6	6.7	6.3	14.1	23.7	24.4
min	1.0	1.6	3.3	10.5	5.0	2.5
max	32.0	29.2	33.3	62.0	84.5	88.5

Table A-5

Cube Directional Ultrasound Velocity

	SOS_ML (m/s)	**SOS_SI** (m/s)	**SOS_AP** (m/s)	**BV_ML** (m/s)	**BV_SI** (m/s)	**BV_AP** (m/s)
1152L	1479.5	1479.0	1491.0	1473.5	1470.5	1527.5
1181R	1485.0	1481.5	1502.5	1500.0	1483.0	1591.0
1189R	1489.5	1490.0	1479.0	1530.5	1531.5	1467.0
1194R	1480.0	1479.0	1488.5	1472.0	1470.5	1513.0
1197L	1478.0	1478.5		1466.0	1469.5	
1203R	1489.0	1492.5	1525.0	1522.5	1538.5	1733.0
1293R	1478.5	1479.0	1488.0	1466.0	1469.0	1509.5
1298R	1480.5	1480.0	1482.5	1477.0	1474.0	1485.0
1309R	1483.5	1485.5	1485.0	1492.5	1497.0	1500.0
1317R	1480.5	1483.0	1486.0	1478.0	1487.0	1507.0
1328R	1478.5	1479.0	1490.5	1466.0	1468.0	1525.5
1337L	1487.5	1495.0	1492.0	1511.0	1545.0	1547.5
1378L	1482.0	1485.0	1485.5	1484.0	1497.5	1500.5
1386L	1482.5	1493.0		1487.0	1535.0	
1407L	1477.5	1479.0	1491.0	1465.5	1471.5	1527.0
1412R	1477.0	1477.0	1477.0	1462.5	1462.5	1457.5
1422L	1479.0	1480.5	1486.0	1472.0	1477.5	1503.0
1429R		1491.0	1522.0		1539.0	1766.5
1460R	1490.5	1484.0	1520.5	1530.5	1498.5	1699.0
1465L	1485.0	1495.0	1508.0	1496.5	1548.5	1611.5
mean	1480.5	1484.3	1494.4	1487.0	1496.7	1553.9
sd	4.3	6.2	14.8	22.5	30.7	91.1
min	1477.0	1477.0	1477.0	1462.5	1462.5	1457.5
max	1490.5	1495.0	1525.0	1530.5	1548.5	1766.5

Table A-6

Cube Trabecular Morphology

specimen ID	BV/TV (mm^3/mm^3)	BS/TV (mm^2/mm^3)	Tb.Th (mm)	Euler conn. ($1/mm^3$)	Tb.N (1/mm)	Tb.Sp (mm)	DA (mm/mm)
1152L	0.2018	13.7854	0.1451	-0.2252	1.3910	0.5739	1.332
1181R	0.3573	11.5057	0.1739	-0.4829	2.0554	0.3127	1.345
1189R	0.2917	10.6904	0.1871	-0.2659	1.5592	0.4543	1.329
1194R	0.2941	12.0823	0.1656	-0.5899	1.7766	0.3973	1.210
1197L	0.3096	14.0791	0.1421	-0.3404	2.1794	0.3168	1.240
1203R	0.5286	7.5136	0.2662	-0.6981	1.9858	0.2374	1.322
1293R	0.3107	13.1020	0.1527	-0.3559	2.0354	0.3387	1.267
1298R	0.3465	12.6470	0.1582	-0.4624	2.1910	0.2983	1.220
1309R	0.3079	13.2679	0.1508	-0.3848	2.0426	0.3389	1.415
1317R	0.3052	13.3204	0.1502	-0.3179	2.0328	0.3418	1.416
1328R	0.2170	12.4834	0.1602	-0.1772	1.3544	0.5781	1.339
1337L	0.4659	10.0953	0.1981	-0.7333	2.3518	0.2271	1.320
1378L	0.3789	11.9340	0.1676	-0.5893	2.2610	0.2747	1.340
1386L	0.5107	8.9698	0.2230	-0.6576	2.2904	0.2136	1.374
1407L	0.2905	13.4365	0.1489	-0.4551	1.9516	0.3636	1.261
1412R	0.1840	16.9054	0.1183	-0.1031	1.5554	0.5247	1.111
1422L	0.3415	12.4741	0.1604	-0.6451	2.1300	0.3092	1.226
1429RB	0.3481	12.6260	0.1584	-0.511	2.1976	0.2967	1.241
1460R	0.2957	11.9127	0.1679	-0.3364	1.7612	0.3999	1.344
1465LB	0.3771	9.8319	0.2035	-0.3859	1.8538	0.3360	1.418
mean	0.3331	12.13	0.1699	-0.4359	1.948	0.357	1.299
sd	0.09	2.04	0.03	0.18	0.30	0.11	0.05
min	0.1840	7.51	0.1183	-0.7333	1.354	0.214	1.111
max	0.5286	16.91	0.2662	-01031	2.352	0.578	1.418

Table A-7

Cube Mechanical Properties

	AP modulus (MPa)	**SI modulus** (MPa)	**ML modulus** (MPa)	**AVG modulus** (MPa)	**Ultimate Stress** (MPa)
1152L	693	127	110	310	1.396
1181R	222	159	95	159	2.615
1189R	184	63	94	114	1.204
1194R	200	119	24	114	0.568
1197L	162	39	25	75	0.391
1203R	425	249	106	260	3.367
1293R	135	39	48	74	0.536
1298R	400	70	89	186	0.862
1309R	663	66	53	261	1.700
1317R	131	141	59	110	0.179
1328R	160	59	13	77	0.494
1337L	720	342	155	406	2.735
1378L	341	120	52	171	0.187
1386L	238	196	278	237	2.610
1407L	185	24	35	81	0.641
1412R	11	8	5	8	0.101
1422L	228	91	64	128	0.810
1429RB	357	91	55	168	2.084
1460R	250	122	256	209	2.969
1465LB	440	234	89	254	1.981
mean	307	118	85	170	1.772
sd	198	84.5	72.4	96.7	1.05
min	11	8	5	8	0.101
max	720	342	278	406	3.367

Appendix B - Standard Operating Procedures and Protocols

Beth Israel Hospital
Orthopaedic Biomechanics Laboratory
Standard Operating Procedure

CALCANEAL ULTRASOUND ANALYSIS OF CADAVER FEET

OBL # IA_U_1, Version #2
Dec 21, 1994

Written by: TR Toledano, ML Bouxsein
Responsibility of: Mary L. Bouxsein
Laboratory Director: _____

Summary: This SOP outlines the protocol for operation and maintenance of the Walker Sonix UBA 575+ Ultrasonic Bone Analyzer (Walker Sonix, Worcester, MA, phone # 508-752-1653) for use in calcaneal ultrasound analysis of cadaver feet.

Key words: ultrasound, walker sonix

Introduction

The UBA 575+ is an ultrasound device which can be used to measure ultrasound attenuation (BUA), transit velocity (SOS), and bone velocity (BV) as it passes through the calcaneus of a live or cadaveric subject. Before beginning the protocol, it is recommended that you consult the UBA575+ User's Manual to understand the setup of the apparatus and the variables measured by the ultrasound scan.

Since you will be using human cadaveric materials, **you must take appropriate steps toward infection control.** It is recommended that you first receive the hepatitis vaccination series and take care to follow all the standard OBL procedures for working with human tissue (SOP #TP1, June 18, 1992).

PRELIMINARY PREPARATION

Checklist of necessary items:

UBA575+ scanner
water
specimens
lab notebook

bleach
saran wrap
gloves, gown, shoe covers
chux
"ALL" detergent
large ziploc bag
plastic tub
Walker-sonix acoustic bone standards

A. SPECIMENS

1) **Thaw time**: Remove each foot from the freezer and thaw it for approximately **18 hours at room temperature**. During thawing, the foot should remain in its sealed plastic bag.

2) Before scanning a foot, soak it for at least 2 minutes in a plastic bag filled to ankle level with soapy water, in order to relieve excess dryness.

B. SCANNER PREPARATION

1) **Cover the keyboard** with Saran Wrap.

2) Turn the computer and screen power on and **allow approximately 10 minutes for the unit to "warm up"** before beginning to test.

3) Slide the blue water tray out from under the scanner. Fill the tray with **room temperature water that has been sitting out for at least 4 hours** (a prepared container of this water is usually found on the ultrasound cart).

4) Add approximately 3 tablespoons of detergent to the water dish. The "All" brand is recommended.

5) Make sure the white knob just above the water tray is pushed in, to prevent water from leaking out of the scanner back into the tray. Empty the blue water dish into the scanner tank. Replace the water dish under the scanner.

6) Line the walls of the scanner tank with Saran wrap, to ease cleanup after the testing has been completed. **Do not cover the transducer openings.**

7) Press enter to continue.

C. SCANNING THE PHANTOMS (**A**coustic **B**one **S**tandards)

Before beginning to scan the actual cadaveric feet, you should perform scans of two phantom "Acoustical Bone Standards" (one red, one blue) provided with the instrument.

The red phantom simulates attenuation in bone of low bone mass. (Expected BUA values range from 25 to 40). The blue phantom simulates attenuation in bone of high bone mass. (Expected BUA values range from 65 to 85). The standards are stored in the plastic case provided by Walker-Sonix and stored on the shelf in the sports medicine / bone densitometry room.

1) From the main menu, select System Maintenance; press enter.

2) Select Test Bone Std; press enter.

3) Select color of the standard you want to test (red, blue).

4) You will be asked to confirm the serial number on the top of the standard. If the numbers do not match, press N, enter the new bone standard serial number, then press F2 to continue. If the numbers match, press Y.

The number for our red phantom is R93045A, and the number for our blue phantom is B920710A.

5) The Water Settling Timer will appear on the screen, marking the start of a 3-minute waiting period. Press "control X" to bypass the waiting time.

6) The computer will then conduct an Ultrasound Self Test.
If the test fails, the screen will give you instructions as to how to proceed.
If the test is successful, the Prepare Bone Standard screen will appear, along with the instruction to place the standard in the scanning tank.

7) Place the standard in the middle of the tank with the arrow pointing toward the knob. Press enter.

8) The computer will then conduct the Scanning System Self Test. When the test is completed, leave the standard in the water and wipe the transducers and sides of the standards gently. Press enter.

9) The computer will then perform the Heel Sequence Scan for the phantom. When the computer has finished with the standard test, the final BUA value will appear on the screen. Record the BUA value in your lab notebook.

10) Press enter. You will see a graph of the BUA values recorded for this phantom on specific dates. If you notice significant inconsistencies in the plot, check the position of the phantom, readjust, and rescan. If there are no major discrepancies, press quit.

11) Press escape to get to main menu.

12) Repeat steps 1 to 11 for the second phantom.

SCANNING THE CADAVERIC SPECIMENS

1) Highlight Scan Patient from the Main Menu on the screen; press enter. The Prepare Scanner screen will appear.

2) Press enter to continue; press control X to bypass the water settling time.

3) The computer will then perform the Ultrasound Self Test. If the test is successful, the Prepare Patient screen will appear, along with the instruction to place the foot in the scanner. If not successful, read the error message, consult the User's Manual and then proceed by trying the Ultrasound Self Test again after making the appropriate changes.

4) Remove the foot from the soapy water it had been soaking in and place it in the scanner such that the calf rests on the back of the scanner tank. Keep the foot centered in the tank, with the heel positioned in the indentation at the bottom of the tank.

5) Wipe the sides of the foot and the transducers with your (gloved) fingers, in order to remove unwanted air from the water.

6) After positioning the foot, press any key to continue.

7) **The Patient Record**: There are several categories of information (name, DOB, sex, identification number) you must provide before you can begin testing.

Enter the patient's last name (or specimen ID). Press enter.

8) The computer will then search its database for a name match. If the specimen has never been scanned before, highlight New Patient on the screen. Otherwise, choose the corresponding patient name and enter the appropriate information required for each sample. The following scheme has been chosen for registering the foot samples:

Last name: FOOT_ _ _ _
First name: right/left
ID#: FT_ _ _ _ R/L (ex: FT1006R)
DOB: from cadaver information sheets
Sex: from cadaver information sheets

Once the patient information is complete, continue the test by pressing F2.

9) **Scanning System Self-Test**: The computer will now perform this test automatically. If the scanning cannot proceed for some reason (e.g. electronic

drift, too much air in water), the screen will give you instructions on how to proceed. If the test succeeds, gently wipe the transducers and sides of the foot again.

11) The computer will now automatically perform the **Heel Scan Sequence.** While the UBA conducts the scan, the computer screen will show a grid of 9 boxes. When all 9 boxes are colored, the scan has been completed for that foot.

12) **Scan results**: The Heel Scan Results screen will appear after completion of the heel scan. The screen will provide a summary of the test results, including the sample name, BUA, Velocity(bone), and SOS. In your lab notebook, the following data should be recorded for each foot:

Name
ID
BUA
SOS
BV

Press any key to continue.

13) You will have the option to print the report or to quit.

14) NOTE: If further information is desired, the UBA575+ has other options for acquiring additional data (Purvis, DDM, Image+, Orchid).

CLEANUP AND MAINTENANCE

1. Keep your gloves on!!!

2. Release the knob underneath the scanner, to release the water from the tank.

3. Clean the tank and tray with a 1:3 solution of bleach:water. **Do not forget to clean all surfaces you may have touched**. Return the scanned feet to their appropriately labelled bags, and return them to the freezer.

Beth Israel Hospital
Orthopaedic Biomechanics Laboratory
Standard Operating Procedure

DUAL ENERGY X-RAY ABSOBTIOMETRY OF THE CALCANEUS

OBL SOP #IA_D_10
1/1/95

Written by: Kendrick Boardman
Responsibility of: Ann Magner
Laboratory Director: _____

Summary: This SOP describes the methods used to scan and analyze the cadaveric calcaneus using the QDR-2000*plus* bone densitometer.

Key words: BMD, calcaneus, DXA

Checklist:
foot holder
short velcro straps
long velcro straps
surgical chucks
QDR-2000
gloves
plastic wrap
ruler (inches)
a marker

PROCEDURE

1. Thaw feet for twelve hours before beginning procedure. The feet do not need to be completely thawed, only pliable enough to flex the ankle.

2. Prepare QDR-2000*plus* for scanning. Remove the gray pad from the scanning table and cover table liberally with surgical chucks. At this time also cover the keyboard with plastic wrap.

3. Draw two lines on the chucks using the black tape on the table as guides. (Taping the chucks to the table can be helpful so that they don't move.)

4. Place foot in foot holder. The longer arm of the holder (the one that extends past the other) is the one that holds the ankle. When properly positioned, the foot will appear to be wearing high heels

5. Use the properly fitting velcro straps to hold the foot in place on the foot holder. Make sure that the heel is snug in the corner and the foot angle is the same as the holder angle. Use the strap holes closest to the heel if possible.

6. Place the foot, lateral side up, on the table with the corner of the foot holder on the intersection of the lines on the chucks and the foot facing towards the head of the table.

7. The foot should be positioned so the calcaneus is approximately parrallel with the long axis of the table. The calcaneus extends from the heel up and into the foot. This means that the calcaneus will not be parrallel with either arms of the foot holder. A best guess estimate of the angle with respect to the centerlines is as accurate as is neccassary.

8. Draw lines on the chucks along both arms of the foot holder. These lines can be used to repostition feet for repeatability trials, and for consistent testing postitioning. **Note**: while all left feet will be postioned identically, and all right feet will be positioned identically, right feet and left feet will be positioned as mirror images of each other.

9. If the QDR-2000 is not turned on, turn it on at this time and enable the x-ray. Turn on the computer controller.

10. Enter the patient into the database.
    10.1 - Select <Patient> from the menu
    10.2 - Select <insert>
    10.3 - Enter the specimen name and type your initials in the scan code box.
    10.4 - Hit <F10> when complete

11. Set up computer for the scan.
    11.1 - Select <scan> from the menu
    11.2 - Select <wrist>
    11.3 - Select <Single Beam Left Wrist> regardless of the anatomical side of the foot.

12. By using the button on the scanning arm, position the laser light half an inch beyond the heel of the foot holder approximately on the center line of the calcaneus.

13. Measure the foot in inches.
    13.1 - The length is measured from the laser to approximately the other end of the calcaneus. This is not a precise measurement and the only goal is to make sure that the scan will contain all of the calcaneus.
    13.2 -.The width measurement should contain all of the calcanesus and the foot holder for approximately half the length of the scan.
    13.3 - Enter the values in the computer in the appropriate boxes.
    13.4 - Record these values along with the point resolution and the line spacing in your laboratory notebook.

14. Press <F10> to begin scan. The "x-ray-in-use" light on the QDR-2000*plus* will light up and a sign on the computer screen will remind you that the x-ray is on. STAY AT LEAST ONE METER AWAY FROM THE SCANNER ARM WHILE THE X-RAY IS ON.

15. Watch the computer screen as the foot is being scanned. If the scanning image does not contain the entire bone or both arms of the foot holder, hit <F3> to rescan.
    15.1 - Reposition the laser by using the cursor buttons to move the blue arrow on the monitor to the desired centered position.
    15.2 - Remeasure the length and width and change accordingly (on the computer and in your notebook)
    15.3 - Hit <F10> to begin the scan again.

16. The scan ID number will appear as the specimen is being scanned. Record this number in your notebook.

17. When the scan is complete, the computer will beep and it will be safe to remove the foot from the holder.

ANALYSIS

NOTE: If scanning a large sample of feet, it is best to analyze the scans at one time after completing all scans so the analysis is consistent.

NOTE: The following is a basic list of keys used in analyzing scans, a complete list and more details about analyzing can be found in the QDR-2000*plus* manual.

Cursor Keys => move selection
Ctrl-Page up => moves selection in smaller increments
Ctrl-Page down => moves selection in larger increments
Insert => selects entire box
Page up => selects the top and left sides of box
Page down => selects the right and bottom sides of box

1. Select <Patient> from the main menu.
   1.1 - select the desired scan from the list.

2. Select <Analyze> from the main menu.

3. Select <Compare> from the menu. Select "Analysis, Foot" from list of scans.

3. Positioning "area of interest" boxes. Note, it is often necassary to hit <enter> and then use the cursor keys to adjust the contrast in order to see the foot holder on the screen image.
   3.1 - Position the top line so that it intersects the center of the arcs on the calcaneus (see Analysis, Foot scan)..
   3.2 - Position the other three points so that the entire end of the calcaneus is enclosed.
   3.3 - Postition the circle on the calcaneus by using the template. Align the arms of the template with the arms on the scan. Then align the circle on the screen with the circle on the template.
   3.4 - When completed, hit <end>

4. Highlight the bone
   4.1 - At this point the calcaneus within the box should be highlighted yellow. If not, use the appropriate keys to insert yellow so it covers all of the bone, but not the soft tissue or holder.
   KEYS: INS => Will highlight the bone(small box is yellow)
   DEL => Will unhighlight the bone (small box is blue)
   shift-PG DWN => Will make the highlighting box smaller
   shift-PG UP => Will make the highlighting box bigger
   4.2 - Press <end> when done.

5. Analysis should be complete, press <Print Screen> for a hardcopy.

6. Press escape for the main menu.

ARCHIVE

1. Select <archive>

2. Select <archive> again

3. Select <1st Optical>, the first optical should be in the drive.
    3.1 - selct files you wish to save with a <+>.
    3.2 - Record disk number and file number in your notebook.

4. Repeat steps 1 to 3 except this time select <floppy> instead of the optical drive.
    4.1 - Insert Floppy disk.
    4.2 - Select files with the <+> key.
    4.3 - Record disk number and file number in your notebook.

5. Store the floppy disks in a safe place, these contain your original data.

Beth Israel Hospital
Orthopaedic Biomechanics Laboratory
Standard Operating Procedure

Determining Average Bone Density of a Circular Region of Interest using Computed Tomography

OBL #IA_Q_6, Version # 1
1 June 1994

Written by: S. E. Radloff
Responsibility of: M.L. Bouxsein
Laboratory Director: W. C. Hayes

Summary: This SOP describes how to determine equivalent mineral density in a circular region of interest on a single slice of a QCT scan.

Key Words: QCT, density

This SOP assumes that the bone specimen(s) of interest have been imaged using QCT, and that the images have been downloaded from the optical disk to the users' directory on the Sun workstation system. The QCT image files should be in *.sht form.

1. Start AVS by typing **avs &** at the unix prompt. Currently, only obl4, obl5, and obl6 have licenses to run AVS. Select **Network Editor** when AVS has loaded.

2. Select **read network** and load the network **density.net** from the **/home/dam/networks** directory.

3. Replace the image viewer module. (This is required because of a glitch in AVS. Directions below taken from OBL SOP Predicting Failure of the Proximal Femur from CT.)

   4.1 Find an imageviewer module by clicking on **Supported** on the top of the screen. Search for it in the **Output** window and drag it down onto the screen.

   4.2 Disconnect the pipe(s) from the old imageviewer by selecting its insertion with the right mouse button and following it to its origin and then letting go.

   4.3 "Trash" the old module by dragging it over to the hammer on the lower right hand corner of the main AVS window.

4.4 Connect the pipes from the new imageviewer exactly the way the old image viewer was connected using the middle mouse button.

4. In the window titled "AVS page.0", referred to here as the control panel, select the correct directory and image file(s).

5. Input the correct mm/pixel conversion in BOTH locations on the control panel. The conversion is: **mm/pixel = FOV/512**, where FOV is the field of view used when the bones where scanned. (eg. 180mm / 512 = 0.3516 mm/pixel.)

6. Depending on the application, you may want to lower the threshold value. (For determining density of the calcaneus, I changed the threshold from 0.2 to 0.05.)

7. Determine the average intensity of each phantom tube.
   7.1 Set the diameter of the circular region of interest. For determining the average intensity, 10 mm works well.
   7.2 Click with the left mouse button on the center of the darkest phantom tube. A circle with the set diameter will appear in the display image window. The average intensity of the image within the circle will appear next to the heading Channel 0: in the values box of the control panel. The circle should be completely inside the phantom tube, otherwise the intensity value will be affected by the surrounding image. This is important!
   7.3 Input the intensity value into the list on the control panel, where D 0mg CT num represents the intensity of the least dense, or darkest phantom.
   7.3 Repeat 7.2 and 7.3 for all 6 phantom chambers.

8. When the intensity of each phantom tube has been set, the diameter of the region of interest circle can be changed to any desired value. To evaluate equivalent mineral density, select the center of the circular region of interest on the image viewer window with the mouse. The average density of bone (or tissue) within the circle is shown in the density box on the control panel. Record the density value and the diameter of the circle in the lab notebook.

Beth Israel Hospital
Orthopaedic Biomechanics Laboratory
Standard Operating Procedure

Predicting Failure of the Proximal Femur from Computed Tomography

OBL Version #IA_A_1
2/14/94

Written by: Daniel Michaeli
Responsibility of: John Hipp
Laboratory Director: Wilson C. Hayes

Summary: This protocol describes methods to obtain geometric and density measurements from CT. This protocol assumes that the CT data have already been converted to short integer arrays. Procedures for converting the original CT data to short integer format are described in other protocols. This report further assumes the reader wants to compare one data set to its contralateral side or two exams of the same bone. To measure density from CT you must first convert the original CT data [which represents X-Ray attenuation in Houndsfield units(HU)] to bone density. This is accomplished using a phantom. The phantom consists of several chambers containing materials of increasing density. The phantom is used to obtain the slope and Y-intercept of a line which converts HU to bone density. Once the CT data have been converted to bone density, several quantitative measures can be obtained for each cross section including: total cross sectional area of bone (above a selected density); average bone density; axial rigidity (this is an estimate of the structural stiffness of the bone under axial loads); and bending rigidities (estimates the bending stiffness of the bone). A user defined subregion of the CT image can be defined to isolate a particular bone. The analysis must be run from a machine that has a license to run AVS (obl4, obl5, obl6).

Key Words: CT, axial rigidity, AVS

note: The protocol was written under the assumption that it was to be used as an entire piece. Because of this the directions assume that the user knows how to do the tasks already explained.

NOTE ON CT DATA

For this procedure, it is best to be consistent when collecting CT scans. The procedure will be simplified if the scans are made with a constant field of view, similar orientation, and equal slice separation.

DETERMINE PARAMETERS

1. To complete the quantitative analysis, several steps must be completed. These steps include: determine the pixel size and slice separation for the images; compute the interpolation factor; determine the centers of each phantom chamber in the first and last slice (see Boundary Definition 3.).
   1.1 The pixel size can be obtained by dividing the field of view (FOV) used when the bones were scanned by the matrix size (eg. 240mm / 512= 0.46875 mm/pixel), or it can be obtained from the files generated when the original CT files were processed (see appendix for references to the protocol appropriate to the manufacturer of the CT scanner you used).
   1.2 The slice thickness and slice separation were defined when the bones were originally scanned. You can recall this information from your notebook, or in some cases you can get the information from the files generated when converting the original files to short integer format.
   1.3 The interpolation factor can be found by dividing the slice separation by the pixel size (e.g. 3mm / .46875mm/pixel=6.4). This number will be needed later in an AVS module. Since the AVS module can not input an interpolation factor greater than 4, two interpolations must sometimes be used (e.g. 6.4 / 4=1.6, interpolation factors are 4, 1.6).

BOUNDARY DEFINITION

1. Load an AVS network
   1.1 On obl4, 5, or 6, type avs at the Unix prompt.
   1.2 Click on **Network Editor** with the left mouse button.
   1.3 Hit the **Read Network** button with the left mouse button.
   1.4 Select **QCT_setup.net** from the browser.

2. Determine the outermost boundary of CT slices.
   2.1 Left click on the **load shts** module and then select the directory containing the files.
   2.2 Select the file you wish to load by searching through the browser.
   2.3 Once the file is on the screen you can translate its position in the imageviewer by pressing on the right mouse button (in the imageviewer) and moving back and forth. You can zoom the image by moving the cursor to the center of the image and holding the shift key while hitting the center mouse button. This will cause the image to expand. You may contract the size of the image by following the same procedure but initially placing the cursor on the edge of the image.

3. Determine the coordinates of the center of each of the phantom chambers.

3.1 In some cases, not all of the chambers will have been captured by the exam. The chambers appear as circles of different brightness. The darkest one is the lowest density, and the brightest one is the highest density.
3.2 While holding down the left mouse button, drag the cross-hairs that appear on the image to the center of a phantom chamber and release. The coordinates of the center of that chamber will appear in one of the small windows on the screen. The CT number will also appear in this box labeled "Channel 0:". You can identify which chamber you are working with by this number. The following table lists the actual density of each chamber for *solid phantoms* and the range of CT numbers that may be found.

Actual Density (gm/cc)	Approximate Range of CT Values
0.0	995-1030
0.05	1030-1140
0.15	1140-1280
0.518	1500-1720
56	2270-2500
1.518	2700-3000

3.3 Determine the coordinates of each chamber and record these numbers.
3.4 Perform steps 2 to 3 for the first and last slice in each scan.

Note: If the cross-hairs do not appear while you click with the left mouse button in the imageviewer, drag the imageviewer to the hammer, drag a new imageviewer from the output menu at the top of the screen (you can scroll through this menu), and reconnect all of the pipes as they appeared before.

DETERMINE REGION OF INTEREST

1. Determine the region of interest in the images that includes only the bone that you want to analyze. In many cases, you will need to complete measurements for several bones in each exam, for instance, the left and right femurs. You need to determine a rectangular region of interest that isolates the single bone you are interested in without including the phantom or other bones. You do this with the AVS **QCT_setup.net** network. If there is more than one bone on the CT slides that you want to use you will have to determine a region of interest for each bone and perform the steps following and including this section.
1.1 Using the file browser in the AVS network **QCT_setup.net** flip through the images in the exam to find the minimum and maximum x and y coordinates which the bone occupies. Note that the minimum and maximum values in a scan may occur on different CT slides. For convenience, round

the coordinates a number that is a multiple of 5 (e.g. 450 instead of 448). Allow extra room to reduce the risk of clipping images.

1.2 Create files required to complete the quantitative analysis. The program (hpslice) that actually does the quantitative analysis requires files containing data that describe the region of interest, the pixel size, the CT number for each phantom, etc. These files are generated by a program (pslice_gen) that determines the CT numbers for each chamber, for each slice. This program (pslice_gen) requires two files, one containing a list of file names, and the second containing the coordinates of the centers of the phantom chambers. The first file must be named **files.lst** and it is created with the command:

ls *.sht >! files.lst

The second file must be called **centers.dat** and it can be created using a texteditor - eg:

edit centers.dat.

This file contains several lines of data which must be in the order/format described below:

Line number(s)	Content	Example
1	pixel size in mm/pixel	0.46875
2	threshold - always = 0	0
3	diameter of the circular region, usually 10	10
4	number of slices in the exam	42
5	number of phantom chambers	6
remaining lines have phantom coordinates	coordinates of centers of each remaining phantom chamber in first and last slices - coordinates for the lowest density chamber should be on the first line xfirst yfirst xlast ylast	332 409 336 412

RUN PSLICE_GEN

1. Run the program to create the parameter files required by the program hpslice. This program requires that the two files **files.lst** and **centers.dat** have been created. This program takes as input the coordinates that define a rectangular region of interest.

1.1 Type the following command at the Unix prompt, substituting your coordinates in:

pslice_gen xmin ymin xmax ymax

2. Check to make sure these coordinates are correct.
   2.1 Load the network **QCT_rect_reg.net**.
   2.2 Enter the directory name containing the sht files, placing a '/' at the end.
   2.3 Enter **sht** for the filename suffix.
   2.4 Enter the **maximum** and **minimum** values for the names of your sht files.
   2.5 Enter the total number of sht files in the **steps** window.
   2.6 Place the min x miny max x max y dials on the correct pslice values.
   2.7 Hit the sleep toggle button. You should see your sht files flipping through 'one by one'. If this doesn't work, check the CONSOLE to see if it is calling the right file (an error will be printed otherwise to the effect of what it thinks you are calling the filename).
   2.8 If the image is cut off at any point, you should adjust the pslice coordinates and then go back to step one of this section.

RUN QUANTITATIVE ANALYSIS

METHOD ONE

Note: This alternative method is to edit the CT images and then to have a batch job run the quantitative analysis. The network **edit_2d** allows you to trace only the parts of the CT file you wish to include and replaces the old files. If you use this network, make sure to have a backup of the sht files!! The advantage of this network is that it assures that each CT file needs to be traced only once (a very time consuming process). If, for instance, one was interested in the effect of different threshold values, the batch file could be run on the same traced images.

1. Edit files to include only desired region.
   1.1 Find the directory and first sht file to be found in the **Filename** browser.
   1.2 Replace the imageviewer.
      a. Find an imageviewer module by clicking on **Supported** on the top of the screen. Search for it in the **Output** window and drag it down onto the screen.
      b. Disconnect the pipe from the old imageviewer by selecting its insertion with the right mouse button and following it to its origin and then letting go.
      c. Connect both pipes from the new imageviewer exactly the way the old imageviewer was connected using the middle mouse button.
   1.3 Zoom in to view one bone on the screen.
   1.4 Closely trace all bones and phantoms one by one with the left mouse button. You should see the tracings appear in the display image window.
   1.5 Hit the output button.
   1.6. Hit anywhere on the screen that is black (preferably on the side).
   1.7 Hit the **reset output** button.

1.8 Load the same short file in again to make sure it was traced properly (as noted previously, you should have a backup if it wasn't)
1.9 Load in the next sht file and preform steps 1.3-1.8 on all sht files.

2. Run quantitave analysis.
2.1 Create text file called 'do_pslice' that looks something like this:

```
\rm *.rig mask*
pslice_gen *** *** *** ***
foreach file (0*.sht)
cat $file.pslice >! pslice.dat
pslice < $file >>! pslice_r.rig
cat mask.byt >>! mask_r.dat
end
```

notes: the pslice coordinates go into the *** locations
'pslice' is replaced by 'hpslice' if solid phantoms were used.
replace pslice_r.rig and mask_r.dat with pslice_l.rig and mask_l.dat if a left bone is being analyzed.

2.2 Type **run do_pslice**
2.3 Such an analysis needs to be done for each bone.

METHOD TWO

1. Run actual quantitative analysis on the defined region.
1.1 Starting AVS in the directory containing your sht files, load the **hpslice.net** network.
1.2 Select a directory for the **Filename** browser and **hpslice.dat fname** browser.
1.3 Enter a **hpslice filename** and a **masked byte** filename (e.g. hpslice_l.out and mask_l.out for left femur). These are the outputs from this network.
1.4 Selecting a sht file in the **Filename** browser and a corresponding pslice file in the **hpslice.dat** fname browser, go through all of the files, one by one starting with the lowest numbered file.
1.5 Trace a region of interest for each sht file and press output when you are satisfied that the region was closely traced. Make sure not to include any phantoms or other bones.
1.6 After the first slide, it is a good idea to check and see that the pslice file is being loaded correctly. If you left click the **hpslice** module, you will see these parameters on the left side of your screen. You can check this against any of your pslice files. (e.g. cat 00504.sht.pslice from Unix command prompt). You should also find the size of the output field by calculating (xmax-xmin)*(ymax-ymin). If you ll (command prompt) the mask file, it should be exactly equal to this number.
1.7 Hit the output button to output the data
1.8 After each slide you should cat the **flist** file that is being created to make sure the slice was added.

1.9 If the module crashes, select **restart same** if given the option. Sometimes, you will not be given this option and 'killing' the process might work.

INTERPOLATE SHT FILES

1. Interpolate the sht files into a three-dimensional field.
   1.1 Create a form file at the Unix command line. (e.g. **pslice2avs 00504.sht.pslice mask.out >! avs.form**.)
   1.2 Load the **interpolate.net** network.
   1.3 Read the form file by hitting **read form** and then selecting it in its directory.
   1.4 Read the browser file (mask file output from script) by hitting the **Browser for File 1** button and then selecting it in its directory.
   1.5 Change the dial values to the interpolation factors calculated previously.
   1.6 Select an output filename (AVS will append a .fld extension on the end).
   1.7 Hit the '**send data** toggle switch. This process could take several minutes depending upon the speed of your computer.

CREATE ISOSURFACE

1. Create a 3 dimensional image of the bone.
   1.1 Load the **isosurface.net** network.
   1.2 Set the read field module to the directory containing the field file just created. Select the file.
   1.3 Disconnect the pipe from the interpolate module to the crop module by selecting its insertion with the right mouse button and following it to its origin and then letting go. This will not let the data go through the computation intensive portion of the network until you are ready.
   1.4 View the file in the imageviewer by moving the knob through the range to see if the short file looks correct.
   1.5 If so, reconnect the pipe in the same way you disconnected it except hold down the middle mouse button.
   1.6 After the data passes to the geometry viewer (this may take several minutes) you will need to adjust the isosurface level and rotate the image.
      1.6.1 The isosurface level should be set to display all of the bone material but not show extra 'jaggedness' (range = 0-20).
      1.6.2 Hit the transform selection button in the geometry viewer module. You can now change the degree of rotation value. Place the mouse in the window and hit the arrow key (on the keyboard) to rotate the bone around the necessary axis.
   1.7 Take a snapshot of this image. This snapshot can be printed or made into a slide.

1.8 Follow this same procedure except set the minimum y or maximum y crop value so that the image is sliced in half in the imageviewer. This should allow you to view the isosurface of the defect in the geometry viewer.

RS1 DATA ANALYSIS

1. The slice output file can be analyzed in any program such as RS1.
   1.1 The values contained in the columns are: total bone area, cortical bone area, trabecular bone area, average density, average modulus, axial rigidity, orientation, max bending moment and min bending moment.
   1.2 The CT files of two femurs (or the same femur scanned at different times) can now be compared by plotting their various parameters on the same graph.

Protocol for cutting trabecular bone cubes from the calcaneus

1. Make a contact radiograph of each foot using the HP Faxitron set at 75 kV for 50 sec.
2. Place the foot in the 105° plexiglass holder, and mark the location of the ultrasound scan on the skin or calcaneus using permanent ink. The location of the ultrasound scan should be determined by using the correct plastic template.
3. Excise the calcaneus from the foot, removing all of the soft tissue from the surface of the bone. If the location of the ultrasound scan was marked on the skin surface, note its location on the calcaneal surface.
4. Glue the calcaneus (3M Scotch-Weld 3535 B/A Urethane Adhesive) to a piece of plexiglass as shown below. The bone should be dry before glue is applied. Draw a line on the plexiglass (perpendicular to the long axis of the calcaneus) indicating where the medial and lateral processes of the calcaneus touch the plexiglass (Figures 1, 2). Also, indicate the right and left sides of the calcaneus on the plexiglass. See *Gray's Anatomy* for a detailed description of the calcaneus.

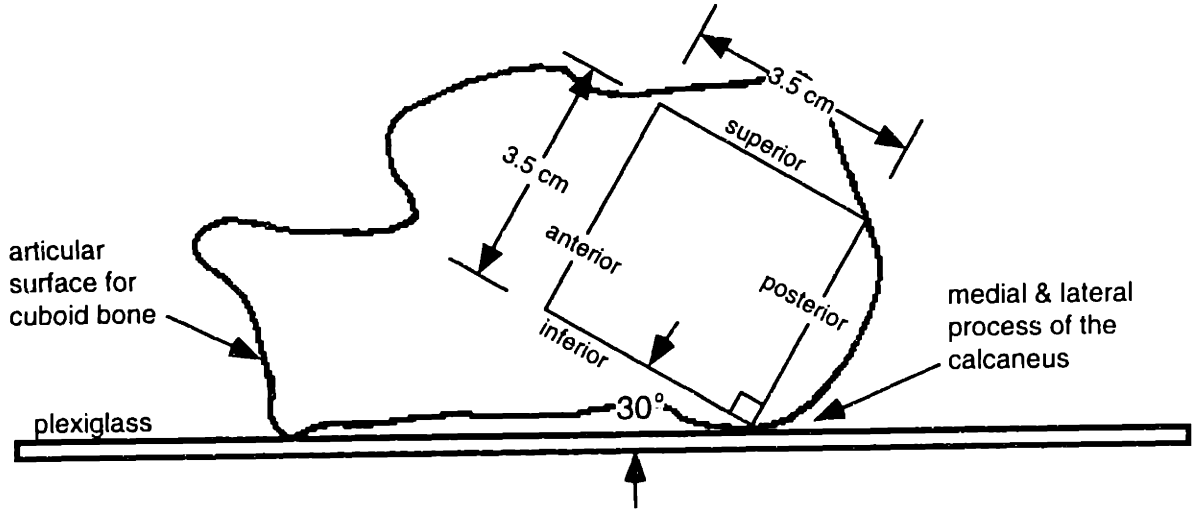

Figure 1 Position of initial bone cut (side view)

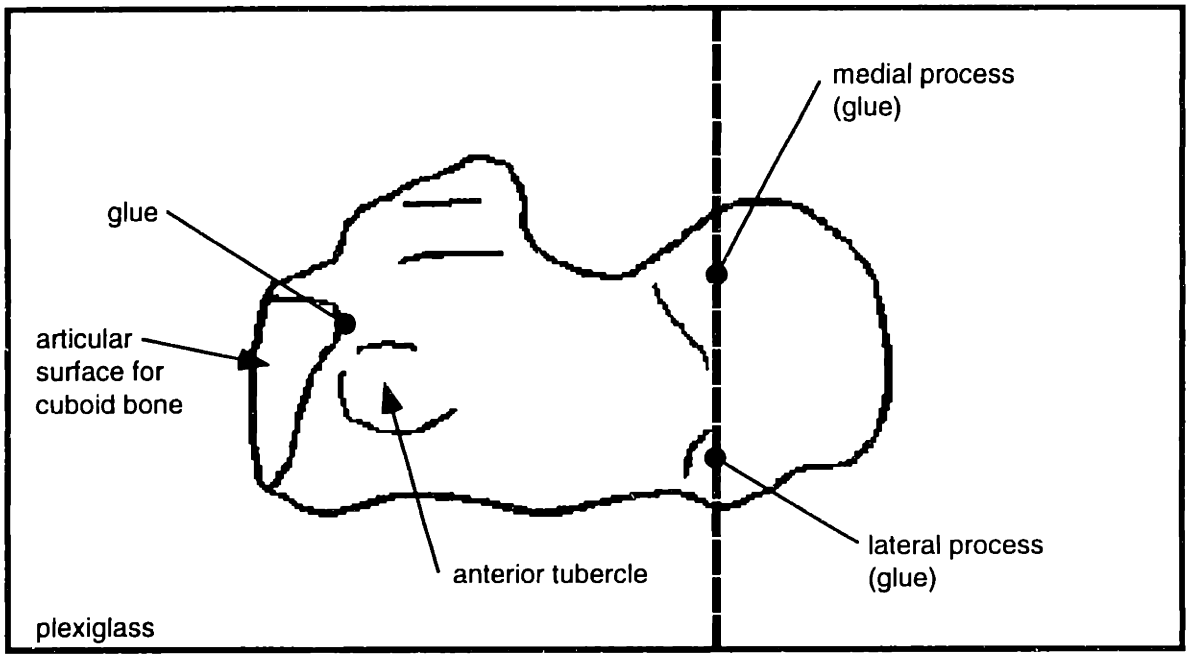

Figure 2 Calcaneus (bottom view)

5. When the glue has dried (after about 45 minutes), embed the calcaneus and plexiglass in rigid foam (Pour Foam, Atlas Industries, Ayer, MA).
    a. Adjust the size of the wooden foam embedding box to fit the bone and plexiglass.
    b. Coat the inside of the box with a thin layer of petroleum jelly.
    c. Place a layer of aluminum foil inside the box. Flatten the foil against the box as much as possible.
    d. Place the bone and plexiglass on the bottom of the container
    e. Measure, in separate containers, 30 cc of each of the foam reactants.
    f. Combine the reactants in a paper cup and stir until the reaction begins.
    g. Pour the foam over the bone and plexiglass. It will slowly expand harden in about 30 minutes.
    h. After it has hardened, remove the bone, plexiglass, and foam from the wooden holder.
6. Cut a 3.5 x 3.5 cm section of bone from the posterior end of the calcaneus (Figure 1) using the band saw in the specimen preparation room. Cut the square at an angle of 30° with respect to the inferior side of the calcaneus. (Thus, the anterior - posterior axis of the cube is aligned with the principal orientation of the trabeculae.) Use a wooden 30-60-90° triangle and the guide attached to the band saw to help maintain the 30° angle when cutting the foam-bone block.
7. Mark the superior edge of the cube with green ink and the anterior/front edge with red ink.

8. Using the contact radiographs of the intact feet and a template similar to the one shown below (Figure 3), locate the position of the trabecular bone cube within the larger square section. The cube should be positioned so that the trabeculae are aligned in the A-P direction, and away from the area of aligned bone at the posterior edge of the calcaneus. Measure the placement of the 15 mm cube with respect to the posterior and inferior surfaces of the large cube and record in the notebook.

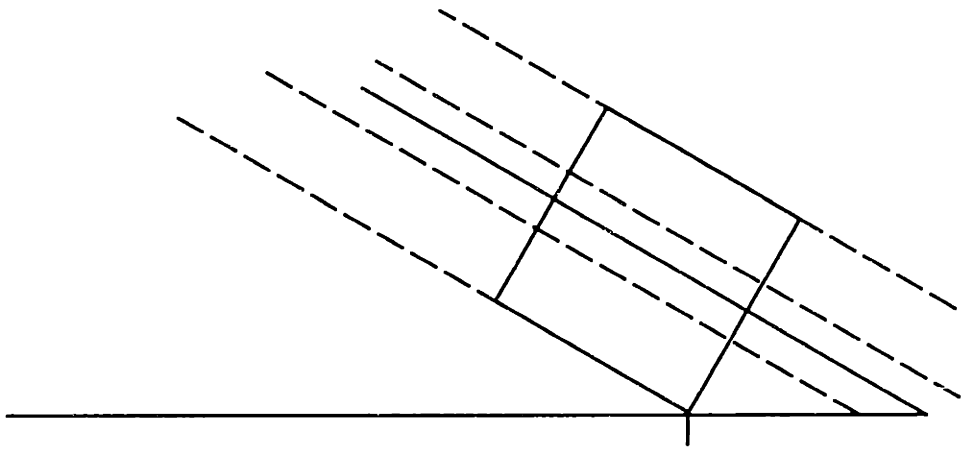

Figure 3 Radiograph cube template

9. Cut a 15 x 15 x 15 mm cube out of the large square section using the Buehler Isomet low speed saw. Set the saw on a speed of 7. To assure that the cut surfaces of the cube are parallel, carefully clamp the bone in the holder in a cantilever beam configuration. Cut one surface, reposition the cube by moving the arm of the saw, and then cut the second surface. DO NOT remove the cube from the holder between cuts of parallel surfaces. Repeat this process for the other 2 directions.
10. Mark the anterior surface of the cube with red ink, the right side with blue ink, and the superior surface with green ink.
11. Wrap the cube in a piece of gauze moistened with saline, seal in a plastic bag, and freeze.

❖

For each specimen, the approximate angle of trabecular orientation was measured from the contact radiograph of the intact foot (Figure 4). The angle was measured with respect to the inferior edge of the calcaneus, as shown in the figure below. The average angle was 30°. Thus, each cube was cut at an angle of 30° with respect to the bottom of the calcaneus.

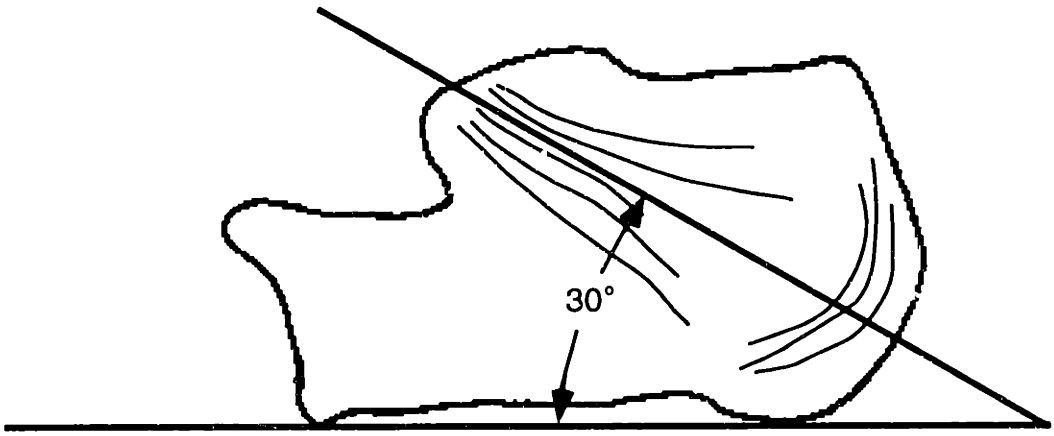

Figure 4 Measurement of trabecular orientation

Beth Israel Hospital
Orthopaedic Biomechanics Laboratory
Standard Operating Procedure

ULTRASOUND SCANNING OF TRABECULAR BONE CUBES

OBL # (to be given) , Version # 1
2 January 1995

Written by: Stefan Radloff
Responsibility of: Mary Bouxsein
Laboratory Director: _____

Summary: This SOP describes the procedure for conducting ultrasound scans of trabecular bone cubes using the Walker Sonix UBA 575+.

Key Words: trabecular bone, ultrasound, QUS, BUA, BV, SOS

This SOP assumes that the reader has a basic familiarity with the Walker Sonix UBA 575+ and knows the procedure for scanning feet in the ultrasound scanner.

SCANNER PREPARATION

1. Add water and detergent to the tank.
2. Save a baseline scan with only water in the tank by selecting System Maintenance => Calibrate Baseline from the menu.
3. Scan both the red and the blue ultrasound phantoms.
4. Place the foam cube bracket in the tank, making sure that the "toe end" of the bracket is on the correct side of the tank.
5. Save the baseline scan once again with the bracket in place.
6. If specific velocity and attenuation data are needed turn on the purvis and ddm programs. To do this, exit to DOS using ctrl-x, type `set purvis = 1` and `set ddm = 1`. Type `runner` to return to the QUS program. Data will be saved on the hard drive as id.asc and id.att files, where id is the scan id given within the QUS setup.

CUBE SCANNING

1. Immerse the cube in saline and degas under vacuum with ultrasonic agitation for at least 30 minutes.

2. Place the cube in the ultrasound scanner. If possible, keep the cube submerged while transferring it to the ultrasound tank. Otherwise, keep the amount of time that the cube is exposed to the air a minimum.
3. Scan the cube in each direction 2 times, repositioning the cube between scans.
4. Wrap the cubes in saline soaked gauze and return them to the freezer when the scanning is complete.
5. Follow the standard procedure for cleaning up equipment contaminated with cadaveric material.

AUA ANALYSIS

1. Copy or ftp the *.att files to a Sun workstation in the /home/ser/aua directory.
2. To calculate aua, type:

```
more file.att | strip > inputfile
aua < inputfile
```

where inputfile is a dummy temporary file.

Appendix C - DXA Output

Orthopaedic Biomechanics Laboratory

k = 1.237 d0 = 132.0(1.000H)

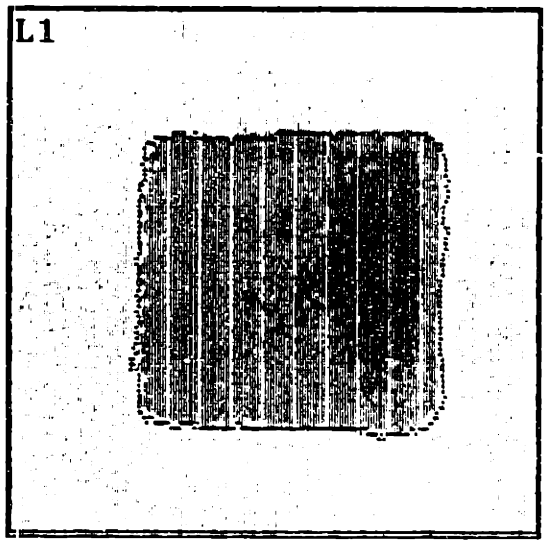

·Aug 10 16:23 1994 [201 x 100]
Hologic QDR-2000 (S/N 2558)
■Lumbar Hi-Res V4.66

C08109426 Wed Aug 10 16:14 1994
Name: CUBE1465L
Comment:
I.D.: Sex: F
S.S.#: - - Ethnic:
ZIPCode: Height: cm
Scan Code: MLB Weight: kg
BirthDate: / / Age:
Physician:
Image not for diagnostic use

TOTAL BMD CV FOR L1 - L4 1.0%

C.F. 1.008 1.084 1.000

Region	Area (cm^2)	BMC (grams)	BMD (gms/cm^2)
L1	2.1049	0.5779	0.2745

HOLOGIC

Appendix D - MicroMRI Imaging Parameters

acqp

```
##TITLE=Parameter List
##JCAMPDX=4.24
##DATATYPE=Parameter Values
##$ACQ_status=( 16 )
<S043>
##$ACQ_protocol_name=( 40 )
<bone_3d>
##$ACQ_method=( 20 )
<se3d>
##$PULPROG=( 16 )
<sehh>
##$GRDPROG=( 16 )
<se3d>
##$ACQ_trim_file=( 16 )
<>
##$ACQ_dim=3
##$ACQ_dim_desc=( 3 )
Spatial Spatial Spatial
##$ACQ_size=( 3 )
400 200 200
##$ACQ_ns_list_size=1
##$ACQ_ns=1
##$ACQ_ns_list=( 1 )
1
##$NI=1
##$NA=1
##$NAE=1
##$NR=1
##$D=( 32 )
0.0965590 0.0027000 0.0001500 0.0009840 0.0000500 0.0010000 0.0012800
0.0000000 0.0000250 0.0000280 0.0598450 0.0000000 0.0000000 0.0025600
0.0000000 0.0000000 0.0000000 0.0000000 0.0000000 0.0000000 0.0000000
0.0000000 0.0000000 0.0000000 0.0000000 0.0204800 0.0000000 0.0000000
0.0000000 0.0000000 0.0000010 0.0020000
##$P=( 32 )
0 32 64 0 500 0 0 0 0 0 0 0 10 0 0 0 0 0 0 0 0 0 0 0 0 0 0 0 0 0 0 0
##$TPQQ=( 8 )
(<sinc2.256>,29.0983,0) (<sinc2.256>,13.5591,0) (<>,10,0) (<>,10,0) (<>,10,0)
(<>,10,0) (<>,10,0) (<>,10,0) (<>,10,0)
##$UL=( 8 )
0 10 11 0 0 0 0 0
##$SW_h=100000.00
##$RG=64
##$SFO1=400.5998400
##$ACQ_O1_mode=BF_plus_Offset
##$ACQ_O1_list_size=1
##$ACQ_O1_list=( 1 )
0
##$O1=0
##$BF1=400.5998400
##$ACQ_flipback=No
##$ACQ_scaling_read=1.0000
##$ACQ_scaling_phase=1.0000
##$ACQ_scaling_slice=1.0000
##$ACQ_grad_matrix=( 1, 3, 3 )
1 0 0 0 1 0 0 0 1
##$AQ_mod=qsim
##$PAPS=AV
##$ACQ_word_size=_32_BIT
##$NSLICES=1
##$NECHOES=1
##$ACQ_fov=( 3 )
1.80 1.80 1.80
```

```
##$ACQ_rare_factor=1
##$ACQ_read_ext=1
##$ACQ_phase_factor=1
##$ACQ_phase_encoding_mode=( 3 )
Read Linear Linear
##$ACQ_spatial_size_1=1
##$ACQ_spatial_phase_1=( 1 )
0.0000000
##$ACQ_phase_enc_start=( 3 )
0 00 -1.00 -1.00
##$ACQ_grad_str_X=27540.6250000
##$ACQ_grad_str_Y=27540.6250000
##$ACQ_grad_str_Z=27540.6250000
##$ACQ_position_X=-0.490
##$ACQ_position_Y=0.360
##$ACQ_position_Z=0.000
##$ACQ_slice_orient=Transverse_Left_Right
##$ACQ_patient_pos=Foot_Supine
##$ACQ_slice_sepn_mode=Contiguous
##$ACQ_slice_angle=( 1 )
0.00
##$ACQ_slice_sepn=( 1 )
0.00
##$ACQ_slice_thick=0.000
##$ACQ_slice_offset=( 1 )
0.000
##$ACQ_flip_angle=0
##$ACQ_obj_order=( 1 )
0
##$ACQ_inter_echo_time=( 1 )
0.000
##$ACQ_recov_time=( 1 )
0
##$ACQ_repetition_time=( 1 )
0
##$ACQ_scan_time=2
##$ACQ_inversion_time=( 1 )
0.000
##$ACQ_time=( 24 )
<18:36:12 16 Sep 1994>
##$ACQ_trigger_enable=No
##$ACQ_institution=( 16 )
<Bruker>
##$ACQ_station=( 16 )
<amx400im>
##$ACQ_sw_version=( 16 )
<940510.B>
##$ACQ_calib_date=( 24 )
<15:10:05 31 Aug 1994>
##$DS=0
##$IN=( 32 )
0.0010000 0.0010000 0.0010000 0.0010000 0.0010000 0.0010000 0.0010000
 0.0010000 0.0010000 0.0010000 0.0010000 0.0010000 0.0010000 0.0010000
 0.0010000 0.0010000 0.0010000 0.0010000 0.0010000 0.0010000 0.0010000
 0.0010000 0.0010000 0.0010000 0.0010000 0.0010000 0.0010000 0.0010000
 0.0010000 0.0010000 0.0010000 0.0010000
##$INP=( 32 )
0 0 0 0 0 0 0 0 0 0 0 0 0 0 0 0 0 0 0 0 0 0 0 0 0 0 0 0 0 0 0 0
##$L=( 32 )
64 -1070656187 -810787464 1076155867 -810787464 1076155867 -810787464
 1076155867 -1039471108 -1071991225 -1039471108 -1071991225 -1039471108
 -1071991225 0 80 764 -487496 0 0 0 1085635584 0 0 0 -1061848064 0 0 0
 -1060102912 0 0
##$DATE=0
##$AUNM=( 17 )
```

<au_zg>
##$CPDPRG=(16)
<waltz16>
##$CPDPRGB=(16)
<mlev>
##$CPDPRGT=(16)
<garp>
##$DL=(8)
10 10 10 10 10 10 10 10
##$DPQQ=(8)
(<>,10,0) (<>,10,0) (<>,10,0) (<>,10,0) (<>,10,0) (<>,10,0) (<>,10,0) (<>,10,0
)
##$DBL=(8)
10 10 10 10 10 10 10 10
##$DBPQQ=(8)
(<>,10,0) (<>,10,0) (<>,10,0) (<>,10,0) (<>,10,0) (<>,10,0) (<>,10,0) (<>,10,0
)
##$TL=(8)
10 10 10 10 10 10 10 10
##$DE=6.2500000
##$DECBNUC=(8)
<off>
##$DECNUC=(8)
<off>
##$DECSTAT=_PO
##$DSLIST=(16)
<>
##$EXP=(16)
<>
##$F1LIST=(16)
<>
##$F2LIST=(16)
<>
##$F3LIST=(16)
<>
##$FL1=0
##$FL2=0
##$FL3=0
##$FL4=0
##$FS=(8)
83 83 83 83 83 83 83 83
##$FW=125000.00
##$HL1=0
##$HL2=6
##$HL3=0
##$HL4=0
##$INSTRUM=(16)
<>
##$LOCNUC=(8)
<2H>
##$NC=0
##$NUCLEUS=(8)
<1H>
##$PHP=1
##$PH_ref=0
##$PR=_11
##$PRGAIN=PG_high
##$QNP=0
##$PW=0.0
##$RD=0.0000000
##$RO=20
##$S=(8)
83 83 83 83 83 83 83 83
##$BF2=400.5998400
##$SFO2=400.5998400

```
##$ACQ_O2_mode=BF_plus_Offset
##$ACQ_O2_list_size=1
##$O2=0
##$BF3=400.5998400
##$SFO3=400.5998400
##$ACQ_O3_mode=BF_plus_Offset
##$ACQ_O3_list_size=1
##$O3=0
##$SOLVENT=( 16 )
<CDCl3>
##$SW=249.626
##$TE=300
##$V9=5.00
##$VCLIST=( 16 )
<CCCCCCCCCCCCCCC>
##$VD=0.0000000
##$ACQ_vd_list_size=4
##$ACQ_vd_list=( 4 )
0.0000100 0.0225000 0.0475000 0.0725000
##$VDLIST=( 16 )
<>
##$VPLIST=( 16 )
<>
##$VTLIST=( 16 )
<>
##$YMAX_a=0
##$YMIN_a=0
##$SEOUT=Broad_band
##$POWMOD=LOW
##$XL=0
##$YL=0
##$ROUTWD1=( 24 )
_0 _0 _0 _0 _0 _0 _0 _0 _0 _0 _0 _0 _0 _0 _0 _0 _0 _0 _0 _1 _1 _0 _0
##$ROUTWD2=( 24 )
_0 _0 _0 _0 _0 _1 _0 _0 _0 _0 _0 _0 _0 _0 _1 _1 _1 _1 _1 _0 _0 _0 _0 _0
##$MSLPARS_f1_select=Proton
##$MSLPARS_f2_select=Decoupler
##$ACQ_digitizer=SLOW_16BIT
##$DR=16
##$MSLPARS_combiner=Off
##$MSLPARS_decoupler=PO_
##$MSLPARS_sttl=( 1 )
LO
##$MSLPARS_preamp_enable=(On,Off,Off)
##$MSLPARS_preamplifier=Proton_Hi
##$MSLPARS_decoupler_level=LO
##$ACQ_receiver=on_F1
##$ACQ_preamp_operation=On_Tune
##END=
```

imnd

```
##TITLE=Parameter List
##JCAMPDX=4.24
##DATATYPE=Parameter Values
##$IMND_method=( 20 )
<spin_echo_3d>
##$Micro_Method=spin_echo_3d
##$Micro_ImageOrientation=xyz
##$Micro_ReadFOV_mm=18
##$Micro_Phase2FOV_mm=18
##$Micro_Phase3FOV_mm=18
##$Micro_NTimePoints=200
```

##$Micro_NPhase2=200
##$Micro_NPhase3=200
##$Micro_AQ_ms=2
##$Micro_Phase_ms=0.984
##$Micro_Slab_ms=0.15
##$Micro_GradDecay_ms=0.055
##$Micro_TE_ms=2.42
##$Micro_TR_s=0.1
##$Micro_ExpTime_str=(16)
<1:6:40.00>
##$Micro_ExpTime_s=4000
##$Micro_NAvg=1
##$Micro_NDummyScans=0
##$Micro_MaxDutyCycle=0.8178078
##$Micro_SweepWidth_kHz=100
##$Micro_RG=64
##$Micro_Pulse180_us=64
##END=

reco

##TITLE=Parameter List
##JCAMPDX=4.24
##DATATYPE=Parameter Values
##$RECO_mode=FT_MODE
##$RECO_inp_order=NO_REORDERING
##$RECO_ft_size=(3)
256 256 256
##$RECO_size=(3)
256 256 256
##$RECO_bc_mode=(3)
RCVR_OFFSET_BC NO_BC NO_BC
##$RECO_dc_offset=(2)
-219 -201
##$RECO_qopts=(3)
CONJ_AND_QNEG NO_QOPTS NO_QOPTS
##$RECO_wdw_mode=(3)
SINE SINE SINE
##$RECO_sbs=(3)
0.000 0.000 0.000
##$RECO_ft_mode=(3)
COMPLEX_FT COMPLEX_FT COMPLEX_FT
##$RECO_pc_mode=(3)
NO_PC NO_PC NO_PC
##$RECO_rotate=(3, 1)
0.0000 0.5000 0.5000
##$RECO_image_type=MAGNITUDE_IMAGE
##$RECO_transpose_dim=0
##$RECO_wordtype=_8BIT_UNSGN_INT
##$RECO_map_mode=PERCENTILE_MAPPING
##$RECO_map_percentile=(2)
0.001 99
##$RECO_map_error=0.00025
##$RECO_globex=(1)
-7
##$RECO_minima=(1)
432
##$RECO_maxima=(1)
395693089
##$RECO_map_min=(1)
-3792
##$RECO_map_max=(1)
6943967
##$RECO_map_offset=(1)
-34947.87444

```
##$RECO_map_slope=( 1 )
3.20967E-05
##$RECO_fov=( 3 )
1.8000 1.8000 1.8000
##$RECO_time=( 24 )
<09:26:18 19 Sep 1994>
##$RECO_abs_time=779981178
##END=
```

Bibliography

Abendschein W, Hyatt GW. Ultrasonics and selected physical properties of bone. *Clin Orthop* 1970; **69**:294-301.

Andre MP, Craven JD, Greenfield MA, Stern R. Measurement of the velocity of ultrasound in the human femur in vivo. *Med Phys* 1980; **7**:324-331.

Anonymous. Consensus development conference: diagnosis, prophylaxis, and treatment of osteoporosis. *Am J Med* 1993; **94**:646-650.

Anonymous. Prevention of hip fractures: A position statement. *American Academy of Orthopaedic Surgeons* 1993;

Ashman RB, Corin JD, Turner CH. Elastic properties of cancellous bone: measurement by an ultrasonic technique. *J Biomech* 1987; **20**:979-986.

Ashman RB, Cowin SC, Van Buskirk WC, Rice JC. A continuous wave technique for the measurement of the elastic properties of cortical bone. *J Biomech* 1984; **17**:349-361.

Ashman RB, Rho JY. Elastic modulus of trabecular bone material. *J Biomech* 1988; **21**:177-181.

Ashman RB, Rho JY, Turner CH. Anatomical variation of orthotropic elasstic moduli of the proximal human tibia. *J Biomech* 1989; **22**:895-900.

Baran DT. Broadband ultrasound attenuation measurements in osteoporisis. *Am J Radiol* 1991; **156**:1326-1327.

Biot MA. Generalized theory of acoustic propagation in porous dissipative media. *J Acoust Soc Am* 1962; **34**:1254-1264.

Biot MA. Mechanics of deformation and acoustic propagation in porous media. *Journal of Applied Physics* 1962; **33**:1482-1498.

Biot MA. Theory of propagation of elastic waves in a fluid-saturated porous solid. *J Acoust Soc Am* 1994; **28**:168-191.

Brown RE. *Ultrasonography: basic principles and clinical applications.* St. Louis: Warren H. Green, Inc., 1975.

Bushong SC, Archer BR. *Diagnostic ultrasound: physics, biology, and instrumentation.* St. Louis: Mosby Year Book, 1991.

Cummings SR, Black DM, Nevitt MC, Browner WS, Cauley JA, Ensrud K, Genant HK, Palermo L, Vogt TM. Bone density at various sites for prediction of hip fracture. *Lancet* 1993; **341**:72-75.

Evans JA, Tavakoli MB. Ultrasonic attenuation and velocity in bone. *Phys Med Biol* 1990; **35**:1387-1396.

Evans WD, Crawley EO, Compston JE, Evans C, Owen GM. Broadband ultrasound attenuation and bone mineral density. *Clin Phys Physiol Meas* 1988; **9**:163-165.

Feldkamp LA, Goldstein SA, Parfitt AM, Jesion G, Kleerekoper M. The direct examination of three-dimensional bone architecture in vitro by computed tomography. *J Bone Min Res* 1989; **4**:3-11.

Gluer CC, Vahlensieck M, Faulkner KG, Engelke K, Black D, Genant HK. Site-matched calcaneal measurements of broadband ultrasound attenuation and single x-ray absorptiometry: do they measure different skeletal properties? *J Bone Min Res* 1992; **7**:1071-1079.

Gluer CC, Wu CY, Genant HK. Broadband ultrasound attenuation signals depend on trabecular orientation: an in vitro study. *Osteoporosis Int* 1993; **3**:185-191.

Gluer CC, Wu CY, Jergas M, Goldstein SA, Genant HK. Three quantitative ultrasound parameters reflect bone structure. *Calcif Tissue Int* 1994; **55**:46-52.

Goulet RW, Goldstein SA, Ciarelli MJ, Kuhn JL, Brown MB, Feldkamp LA. The relationship between the structural and orthogonal compressive properties of trabecular bone. *J Biomech* 1994; **27**:375-389.

Greenfield MA, Craven JD, Huddleston AL, Kehrer ML, Wishko DS, Stern R. Measurement of the velocity of ultrasound in human cortical bon in vivo. *Radiology* 1981; **138**:701-710.

Greenfield MA, Craven JD, Wishko DS, Huddleston AL, Friedman R, Stern R. The modulus of elasticity of human cortical bone: an in vivo measurement and its clinical implications. *Radiology* 1975; **115**:163-166.

Grimm MJ, Chung HW, Wehrli FW, Williams JL. Dependence of ultrasound attenuation on plate separation in trabecular bone. *Proceedings of the Orthopaedic Reserch Society* 1994; 442.(Abstract)

Hagiwara S, Yang SO, Gluer CC, Bendavid E, Genant HK. Noninvasive bone mineral density measurement in the evaluation of osteoporosis. In: Lane NE, ed. *Rheumatic disease clinics of north america: osteoporosis.* Philadelphia, W.B. Saunders Company, 1994:651.

Halliday D, Resnick R. *Fundamentals of physics*. 3rd ed. New York: John Wiley & Sons, 1988.

Hans D, Arlot ME, Schott AM, Roux JP, Meunier PJ. Ultrasound measurements of the os calcis reflect more than the microarchitecture of bone than bone mass. *J Bone Min Res* 1993; s156.(Abstract)

Heaney RP, Avioli LV, Chesnut CH,III, Lappe J, Recker RR, Brandenburger GH. Osteoporosis bone fragility: detection by ultrasound transmission velocity. *JAMA* 1989; **261**:2986-2990.

Holmes JH. Diagnostic ultrasound: historical perspective. In: King DL, ed. *Diagnostic ultrasound*. St. Louis, C.V. Mosby Company, 1974:1-15.

Hosie CJ, Smith DA, Deacon AD, Langton CM. Comparison of broadband ultrasounic attenuation of the os calcis and quantitative computed tomographhy of the distal radius. *Clin Phys Physiol Meas* 1987; **8**:303-308.

Jeffcott LB, McCartney RN. Ultrasound as a tool for assessment of bone quality in the horse. *Vet Rec* 1985; **116**:337-342.

Kaufman JJ, Einhorn TA. Perspectives: Ultrasonic assessment of bone. *J Bone Min Res* 1993; **8**:517-525.

Keaveny TM, Guo XE, Wachtel EF, McMahon TA, Hayes WC. Trabecular bone exhibits fully linear elastic behavior and yields at low strains. *J Biomech* 1994; **27**:1127-1136.

Keaveny TM, Hayes WC. A 20-year perspective on the mechanical properties of trabecular bone. *Trans ASME: J Biomed Eng* 1993; **115**:534-542.

Lang SB. Ultrasonic method of measuring elastic coefficients of bone and results on fresh and dried bovine bones. *IEEE Trans Biomed Eng* 1970; **BME-17**:101-105.

Langton CM, Palmer SB, Porter RW. The measurement of broadband ultrasonic attenuation in cancellous bone. *Eng Med* 1984; **13**:89-91.

Lin D, Xu W, Klein M, Einhorn TA, Kaufman JJ, Siffert RS. Effect of physical factors on ultrasound attenuation and velocity. *J Bone Min Res* 1993; **8**:S319.(Abstract)

Linde F, Hvid I, Madsen F. The effect of specimen geometry on the mechanical behavior of trabecular bone specimens. *J Biomech* 1992; **25**:359-368.

Marks' standard handbook for mechanical engineers. 9th ed. New York: McGraw-Hill Book Company, 1987: 5-82-5-83.

McCloskey EV, Murray SA, Charlesworth D, Miller C, Fordham J, Clifford K, Atkins R, Kanis JA. Assessment of broadband ultrasound attenuation in the os calcis in vitro. *Clinical Sci* 1990; **78**:221-225.

McCloskey EV, Murray SA, Miller C, Charlesworth D, Tindale W, O'Doherty DP, Bickerstaff DR, Hamdy NAT, Kanis JA. Broadband ultrasound attenuation in the os calcis: relationship to bone mineral at other skeletal sites. *Clinical Sci* 1990; **78**:227-233.

McKelvie ML, Fordham J, Clifford C, Palmer SB. In vitro comparison of quantitative computed tomography and broadband ultrasonic attenuation of trabecular bone. *Bone* 1989; **10**:101-104.

McKelvie ML, Palmer SB. The interaction of ultrasound with cancellous bone. *Phys Med Biol* 1994; **36**:1331-1340.

Melton LJ, Kan SH, Frye MA, Wahner HW, O'Fallon WM, Riggs BL. Epidemiology of vertebral fracture in women. *Am J Epidemiol* 1989; **129**:1000-1011.

Melton LJ. Epidemiology of Fractures. In: Riggs BL, Melton LJ, eds. *Osteoporosis: etiology, diagnosis, and management*. New York, Raven Press, 1988:133-154.

Miller CG, Herd RJM, Ramalingam T, Fogelman I, Blake GM. Ultrasonic velocity measurements through the calcaneus: which should be measured? *Osteoporosis Int* 1993; **3**:31-35.

Parfitt AM, Drezner MK, Glorieux FH, Kanis JA, Malluche H, Meunier PJ, Ott SM, Recker RR. Bone histomorphometry: standardization of nomenclature, symbols, and units. *J Bone Min Res* 1987; **2**:595-610.

Rice JC, Cowin SC, Bowman JA. On the dependence of the elasticity and strength of cancellous bone on apparent density. *J Biomech* 1988; **21**:155-168.

Rossman P, Zagzebski J, Mesina C, Sorenson J, Mazess R. Comparison of speed of sound and ultrasound attenuation in the os calcis to bone density of the radius, femur and lumbar spine. *Clin Phys Physiol Meas* 1989; **10**:353-360.

Rubin CT, Pratt GW, Porter AL, Lanyon LE, Poss R. Ultrasonic measurement of immobilization-induced osteopenia: an experimental study in sheep. *Calcif Tissue Int* 1988; **42**:309-312.

Salamone LM, Krall EA, Harris S, Dawson-Hughes B. Comparison of broadband ultrasound attenuation to single x-ray absorptiometry measurements at the calcaneus in postmenopausal women. *Calcif Tissue Int* 1994; **54**:87-90.

Saltykov SA. *Sterometric Metallography*. 2nd ed. Moscow: Metallurgizdat, 1958.

Stegman MR, Travers-Gustafson D, Heaney RP, Recker RR. Comparison of ultrasound and spa for determining odds ratio of low-trauma fracture in post menopausal wome. *J Bone Min Res* 1994; **9**:s329.(Abstract)

Stuessi E, Faeh D. Assessment of bone mineral content by in vivo measurement of flexural wave velocities. *Med Biol Eng Comput* 1988; **26**:349-354.

Taube RA, Adelstein SJ. A short historyof modern medical imaging. In: Guzzardi R, ed. *Physics and engineering of medical imaging*. Bordrecht, Martinus Nijhoff Publishers, 1987:9-40.

Tavakoli MB, Evans JA. Dependence of the velocity and attenuation of ultrasound in bone on the mineral content. *Phys Med Biol* 1991; **36**:1529-1537.

Travers-Gustafson D, Stegman MR, Recker RR, Heaney RP. Ultrasound and spa differences for older women and men with and without a history of low-trauma fracture. *J Bone Min Res* 1994; **9**:s205.(Abstract)

Turner CH, Eich M. Ultrasonic velocity as a predictor of strength in bovine cancellous bone. *Calcif Tissue Int* 1991; **49**:116-119.

Wasnich RD, Ross PD, Heilbrun LK, Vogel JM. Selection of the optimal skeletal site for fracture risk prediction. *Clin Orthop* 1987; **216**:262-269.

Waud CE, Lew R, Baran DT. The relationship between ultrasound and densitometric measurements of bone mass at the calcaneus in women. *Calcif Tissue Int* 1992; **51**:415-418.

Wild JJ, Reid JM. Application of echo-ranging techniques to the determination of structure of biological tissues. *Science* 1952; **115**:226-230.

Williams JL. Ultrasonic wave propagation in cancellous and cortical bone: Prediction of some experimental results by Biot's theory. *J Acoust Soc Am* 1992; **91**:1106-1112.

Wright LL, Glade MJ, Gopal J. The use of transmission ultrasonics to assess bone status in the human newborn. *Pediatr Res* 1987; **22**:541-544.

Zagzebski JA, Rossman PJ, Mesina C, Mazess RB, Madsen EL. Ultrasound transmission measurements through the os calcis. *Calcif Tissue Int* 1991; **49**:107-111.